UNIVERSITY OF CALIFORNIA, SAN DIEGO

Weak Interactions of Hot Nuclei in Stellar Collapse

A dissertation submitted in partial satisfaction of the
requirements for the degree
Doctor of Philosophy

in

Physics

by

Gordon Wendell Misch

Committee in charge:

Professor George Fuller, Chair
Professor Adam Burgasser
Professor Dusan Keres
Professor Kurt Marti
Professor Bernard Minster

2014

ProQuest LLC.
789 East Eisenhower Parkway
P.O. Box 1346
Ann Arbor, MI 48106 - 1346

The dissertation of Gordon Wendell Misch is approved, and it is acceptable in quality and form for publication on microfilm and electronically:

_____

_____

_____

_____

_____

Chair

University of California, San Diego

2014

DEDICATION

To those who persist in struggling forward.

EPIGRAPH

We are made of star-stuff.

—Carl Sagan

$\frac{12+144+20+3\sqrt{4}}{7} + (5 \times 11) = 9^2 + 0$

—Leigh Mercer

TABLE OF CONTENTS

LIST OF FIGURES

LIST OF TABLES

ACKNOWLEDGEMENTS

The phrase "it takes a village" is most commonly applied to the task of raising a child, but there are other endeavors which, while centered around an individual, require the effort and input of many. The completion of my graduate work is such an endeavor, and I would like to thank some of the many here.

First, I want to thank my advisor, George Fuller, who saw me through all of my graduate research. He has provided guidance both scientific and professional, and support both financial and intellectual. Most of all, he gave me a chance when I needed it most.

This brings me to Hans Paar, another individual without whom I could not have completed my Ph.D. at UCSD. He did for me one of the most important things anyone ever has: he listened, and for that, I owe him my career. Along with Hans, I would also like to thank John Sexton, who provided the help that Hans correctly ascertained I needed.

Between tragedy and various looming deadlines promising doom, I have put my doctoral committee through no small amount of rush, and I am grateful for their patience and cooperation.

In completing the work in this thesis, I have enjoyed the benefit of my collaborators, B. Alex Brown and Calvin Johnson. I have also had countless helpful discussions with Chad Kishimoto and JJ Cherry, and Alex Mendez has offered help with computers on numerous occasions. Dana Johnson has always been an indispensable assistance on any matter involving paperwork and tracking people down. There are many others that would rightly belong on this list, and these few represent only the greatest contributors that come immediately to mind.

I would like to acknowledge the National Science Foundation, which funded the grants from which my graduate tuition, fees, and salary were paid.

I have been graced with a passel of friends that have provided companionship, entertainment, and emotional support. I cannot possibly list them all, and some have already been named, but I would like to mention a few in particular. I have enjoyed many hours of gaming with Ian Schanning, Tiffany Poon, Nick & Wendy Alcaraz, Marc & Lauren Rafelski, and the Wednesday Night Magic crowd

in all its incarnations. I have been privileged with the companionship of Hao Ye and Nathan Johnson, who are generally up for anything, and the members of CASS who frequent tea time. All of these people and more contributed to the richness of my life in San Diego.

In no small part do I owe this achievement to my family, who only ever wanted for me my happiness and self-fulfillment. My parents, Gordon and Charlotte, and brother Derek have been with me through every step and misstep of the long journey of my education, giving guidance, encouragement, and comfort. I wouldn't be here without them. I have also enjoyed the support and company of my extended family and stepmother.

Finally, I would like to give my heartfelt thanks to my girlfriend, Alice Shih. Her patience and support have been utterly invaluable. While I was writing this thesis, she relieved me of a great deal of domestic burden. In the few years that I have known her, she has given me ample emotional support, encouragement, and love through many challenges. She has been a constant companion, and my life would be the poorer for her absence.

Chapter 2, in full, is a reprint (with the exception of references, which have been moved to the end of this thesis) of material previously published as G. Wendell Misch, B. Alex Brown, and George M. Fuller, "Neutrino-pair Emission from Hot Nuclei During Stellar Collapse", *Physical Review C* **88** 015807 (2013), 1301.7042. I was the primary investigator and author of this paper.

Chapter 3, in full, is material currently in preparation for publication in an academic journal with co-authors George M. Fuller, B. Alex Brown, and Calvin W. Johnson. I am the primary investigator and author of this paper.

VITA

2006	B. S. in Physics, Washington State University
2006-2010	Graduate Teaching Assistant, University of California, San Diego
2010-2014	Graduate Research Assistant, University of California, San Diego
2014	Ph. D. in Physics, University of California, San Diego

PUBLICATIONS

G. W. Misch, B. A. Brown, and G. M. Fuller, "Neutrino-pair emission from hot nuclei during stellar collapse", *Physical Review C*, 88, 2013.

G. W. Misch, G. M. Fuller, B. A. Brown, and C. Johnson, "Modication of the Brink-Axel Hypothesis for High Temperature Nuclear Weak Interactions", *In Preparation*

ABSTRACT OF THE DISSERTATION

Weak Interactions of Hot Nuclei in Stellar Collapse

by

Gordon Wendell Misch

Doctor of Philosophy in Physics

University of California, San Diego, 2014

Professor George Fuller, Chair

The physics of the atomic nucleus and supernovas are fundamental to our very being. Indeed, supernovas provide the wind that disperses the nuclei of which we are composed, and the physics of nuclei is pivotal in supernova dynamics. During supernova core collapse, the extremely high temperatures and densities and low entropy favor large, neutron-rich nuclei at high excitation energy. My collaborators and I examine two weak interactions that occur in nuclei under these conditions. First, we study the production of neutrino pairs via de-excitation of hot nuclei. In de-exciting, the nucleus can emit a virtual Z^0 boson that decays into a neutrino-antineutrino pair. We find this to be the dominant source of neutrino pairs of all flavors during collapse. Second, we use modern shell model computation techniques to revise the Brink-Axel hypothesis method of computing electron

capture rates that was pioneered by Fuller, Fowler, and Newman. Our results show that the Brink-Axel hypothesis (which posits that the bulk of nuclear transition strength is distributed among transition energies independently of initial excitation energy) fails at low and moderate excitation, but that at high initial energies, the strength is largely independent of excitation. The failure of the Brink-Axel hypothesis manifests as the redistribution of strength to low and negative transition energies, which can have the effect of increasing the overall electron capture rate in the core.

Chapter 1

Introduction

Throughout this work, I will liberally use "natural units," *i.e.*, units such that $\hbar = c = k_B = 1$. These three constants contain the four dimensions of time, energy, length, and temperature, leaving one independent base unit by which to measure all four dimensions. Generally, this usage will not be made explicit, and I will simply give a temperature in mega electron volts (MeV), or an angular momentum will be dimensionless, or the above constants will simply not appear in an equation. When a dimensionful quantity is listed, the units attached to it can be converted by appropriate application of the above constants in units of the reader's choice. Additionally, A will be the atomic mass number of the nucleus, given by the sum of the proton number Z and the neutron number N; this convention will be absolutely invariant, and later sections will freely assume understanding of the meanings of these labels.

I will assume a basic familiarity with quantum mechanics and statistical mechanics, avoiding lengthy discussions on the fundamentals of those topics and only addressing those aspects which are directly applicable.

1.1 Supernovas

As a star with mass greater than $\sim$10 $M_\odot$ (solar masses) evolves, it goes through a series of nuclear fusion ("burning") phases in its core. It begins with hydrogen burning, which causes the buildup of a helium-rich core. Gradually, as it

grows in mass, the helium core contracts and heats until it ignites helium burning, which produces heat and halts the contraction. This process repeats several times with heavier and heavier core elements until eventually, a silicon core burns into iron. Iron, on the other hand, is an extremely tightly bound nucleus, and there is no energy to be gained by fusing it into heavier elements. Thus, as the iron core grows, it becomes denser and denser, held against gravity by the pressure of a degenerate sea of electrons. When the iron core reaches the Chandrasekhar mass of $\sim$1.4 $M_\odot$, the electron degeneracy pressure is no longer sufficient to support the core, and it undergoes a rapid collapse in about 1 second.

1.1.1 Supernova Cores

During the collapse, the core separates into an inner core that falls subsonically and an outer core that falls supersonically. The mass of the inner core is set principally by the electron-to-baryon ratio Y_e; the degeneracy pressure of the electrons tends to slow the collapse, so a larger Y_e yields a larger inner core. All parts of the inner core remain in causal contact, and it collapses self-similarly until it reaches a density of a few times nuclear density, when it stops suddenly and rebounds. The outer core, on the other hand, doesn't know when it's time to stop, as it is falling faster than information about conditions at smaller radii can propagate outward. It consequently piles onto the inner core just as the inner core is rebounding, and this launches a shockwave. The shock propagates outward and is thought to be one of the mechanisms – along with a neutrino wind – that unbinds the star's envelope, blasting it into the interstellar medium. But when this simple picture is modeled in one dimension on computers, the shockwave dissipates its energy by dissociating the nuclei of the outer core. The loss of energy causes it to stall and collapse back down onto the proto-neutron star [1–3].

More recently, the inclusion of multi-dimensional hydrodynamics and more sophisticated nuclear and neutrino microphysics has improved our understanding of the supernova mechanism [4–9], but it remains true that the outer core plays a major role in dissipating the shock energy. We must therefore include in supernova models the best core physics possible, and the physics of the core is to a great extent

the physics of the nucleus under extreme conditions.

1.1.2 Nuclei During Core Collapse

For some of the arguments in this section, it is useful to have a simple model of the nucleus just for the sake of getting an intuitive physical picture. To that end, consider the nucleus as a Fermi gas consisting of two species, to whit, protons and neutrons. The nucleons propagate therein as non-interacting plane waves. The ground state is then the completely degenerate gas, with protons and neutrons filling all states below the Fermi energy of their respective species, and nuclear excitations arise from single particle excitations above the Fermi sea.

At the onset of collapse, the core is extremely dense ($\sim 5 \times 10^9$ g/cm^3) and extraordinarily hot ($\sim$1 MeV). Despite this, the fact that the electrons are degenerate and the nucleons bound up in moderately sized nuclei makes the entropy very low at $\sim$1 k_B per baryon [10]. Naturally, these conditions are opaque to photons, but as the core collapses, neutrinos freely escape until a density of $\sim 10^{12}$ g/cm^3. Various neutrino production processes act to cool the core, keeping entropy low throughout collapse [11–14].

Because of the low entropy, most of the nucleons remain bound in large nuclei. This follows intuitively from the point that a large nucleus has fewer degrees of freedom than many free nucleons or small nuclei, and is made explicit in reference [10], with a typical nuclear mass number being A $\sim$ 100. The high temperature has an interesting effect on large nuclei: the Bethe approximation for the level density of the nucleus [15] predicts a mean excitation energy of

$$E = aT^2 \tag{1.1}$$

where T is the temperature in MeV and a is the level density parameter given approximately by $a = A/8$ MeV^{-1}. This is understood intuitively from a Fermi gas model of the nucleus wherein approximately aT nucleons are excited to energies of approximately the temperature.

With $A = 100$ and $T = 1$ MeV, the mean excitation is $\sim$12.5 MeV, and a temperature of $T = 1.5$ MeV gives an excitation of 28 MeV, which are high

excitations indeed! There are two important points here. The first is that these highly excited nuclei are bound, as we are not exciting just one or two nucleons. This comes from the fundamental postulate of statistical mechanics that all states are equally likely, and there are many more ways to excite several nucleons a little bit above the Fermi surface than one or two nucleons by a lot. The second point is that while the Boltzmann factor $e^{-E_n/T}$ exponentially suppresses the occupation index of state n, the density of states within the nucleus grows exponentially with energy; this rapid growth, seen in Fig. 2.9, competes with the Boltzmann factor, yielding the large excitations.

As the collapse progresses, electrons capture onto free protons and nuclei, reducing Y_e. As the core becomes more and more neutron rich, it becomes less and less energetically favorable for electrons to capture on nuclei, since in the Fermi gas picture of the nucleus, the difference in the Fermi levels of protons and neutrons becomes larger and larger. This causes Pauli blocking of electron capture, as the protons in the nucleus require a large amount of energy to reach the top of the neutron Fermi sea. This effect can be alleviated thermally by the excitation of protons to higher levels (reducing the jump to the neutron Fermi level) and the excitation of neutrons, which leaves behind holes at lower energy that can then serve as final states for electron-capturing protons [16]. As the supernova evolution is sensitive to Y_e, it is then also sensitive to the physics of hot nuclei.

The stage is now set. We have an extremely dense, hot, low entropy environment that favors large nuclei with high excitation energies, and the evolution of the supernova is sensitive to the behavior of those nuclei. The work in the following chapters examines some important aspects of that behavior.

1.2 Nuclear Physics

The atomic nucleus is essentially a droplet of strongly interacting matter consisting of a number of net quarks equal to three times the atomic mass number and a sea of gluons and quark-antiquark pairs. Treating this mess with a rigorous quantum chromodynamics approach is still a distant dream, but it can be effec-

tively described as a much smaller number of quasi-particles with *nearly identical* quantum numbers (including mass, electric charge, spin, isospin, etc.) as bare protons and neutrons. In fact, this approximation is so good that we will continue to think of and refer to them as such.

1.2.1 Spin and Isospin

In the context of nuclear physics, "spin" is commonly used to refer to total the quantum angular momentum of the nucleus, being comprised of the combined spins and orbital angular momenta of its constituent particles; this is in contrast to the more common usage of spin to refer strictly to that part of the angular momentum of a particle which is not derived from orbital motion. In this work, I will use "spin" to refer to the total angular momentum of the nucleus and the intrinsic angular momentum of protons and neutrons (nucleons), and "orbital angular momentum" to refer to the angular momentum of particles due to their motion around a potential. The gory details of quantum angular momentum and the addition thereof are, I think, best left in the textbooks. Here, I will touch on it just briefly as it relates to the topic at hand.

The total angular momentum $\mathbf{J}$ of a nucleon in the nucleus is the combination of its orbital angular momentum $\mathbf{L}$ and spin $\mathbf{s}$. Nucleons have a spin of 1/2, meaning that there are two possible outcomes when it is summed with $\mathbf{L}$ to obtain $\mathbf{J}$: either $\mathbf{L}$ and $\mathbf{s}$ are aligned, giving $J = L + 1/2$ ("stretched"); or $\mathbf{L}$ and $\mathbf{s}$ are anti-aligned, pointing in opposite directions, giving $J = L - 1/2$ ("jackknifed"). The total angular momenta of the nucleons are then summed according to the usual rules to obtain the spin states of the nucleus.

Isospin – short for isobaric or isotopic spin – is a quantum number carried by particles that interact via the strong force. The inclusion of "spin" in the name of this quantity is due to the fact that it is treated mathematically in a manner very similar to the spin of angular momentum. Particles of different charges that interact identically with the strong force can be considered to be different isospin states of the same species. What this means for our purposes is that we have a single species of particle, the nucleon. Each nucleon has a total isospin of 1/2,

with protons being a nucleon with z-projection of isospin $\tau_z = +1/2$ (isospin up) and neutrons being $\tau_z = -1/2$ (isospin down).

With respect to the strong nuclear force, isospin is nearly a good symmetry, which is to say that the strong force treats protons and neutrons identically. It is not *strictly* true that protons and neutrons behave identically in the nucleus, as they have slightly different masses and their different charges and magnetic dipole moments do break the isospin symmetry, and isospin mixing can arise. But the effects of mixing are small [17], and we ignore them.

1.2.2 The Nuclear Shell Model

The nucleus can be considered to consist of protons and neutrons moving in a collective potential well, usually a variant of the Woods-Saxon potential [18] given by

$$V(r) = \frac{V_0}{1 + e^{(r-r_0)/a}} \tag{1.2}$$

where V_0 indicates the depth of the potential, r_0 is the size of the nucleus, and a sets the diffuseness of the nuclear surface. This central potential is built up from the presence of the many nucleons, and in the first order approximation, individual nucleons otherwise move without interaction with one another. The potential gives rise to individual single particle states described by quantum numbers similar to those of the electrons in an atom: they are designated by the principal quantum number n of the radial component of the associated wave function and the orbital angular momentum **L**. The nucleons fill those states starting from the lowest energy and going up – obeying the Pauli exclusion principle – until all nucleons have been placed, yielding the ground state of the nucleus. Excited states of the nucleus are constructed by moving individual nucleons into higher-energy single particle states, much the same as atomic excitations largely result from excitations of single electrons.

There exist in the nucleus certain "magic numbers" (specifically 2, 8, 20, 28, 50, 82, 126) of nucleons that are particularly tightly bound. That is, the energy gap between the n^{th} and the $n+1^{th}$ single particle states is enhanced when n is a magic number, giving rise to the notion of nuclear shells. Protons and neutrons are

counted separately, and a nucleus with a magic number of each is called "doubly magic." However, these numbers cannot be accounted for by the action of the central potential alone, and this is where the nuclear single particle state structure diverges from the electron analogy. Maria Goeppert-Mayer and her collaborators found that a strong coupling between the spin and orbital angular momentum produces the measured magic numbers [19–21], for which work they were awarded the 1963 Nobel prize. Essentially, the single particle nuclear Hamiltonian contains a term proportional to $-\mathbf{L}\cdot\mathbf{s}$, causing the stretched state to be lower in energy than the jackknifed state. This spin-orbit splitting reorders the single particle levels and produces energy gaps where the number of states with energies lower than the gap energy is a magic number; a very nice schematic of this is given in reference [22]. In the independent single particle shell model (ISPSM), non-interacting nuclei occupy these single particle states, which are labeled by nL_J, where n and L are as in the electron analogy, and J is the *total* angular momentum $L \pm s$. As with electron orbitals, the orbital angular momentum L is usually denoted by a letter, with L=0 indicated by s, L=1 by p, L=2 by d, L=3 by f, and higher values of L proceeding alphabetically from f.

The ISPSM is an excellent tool for understanding the gross features of the nucleus. It successfully predicts the ground state spin and parity of nuclei by simply filling the single particle states from the bottom up with the assumption that nucleons in the same sub-shell (same nL_J) will always pair to minimize the total angular momentum, and it was the basis for the works of Fuller, Fowler, and Newman [23–26] (collectively "FFN"), which even today serve as the standard against which computations of nuclear weak rates in a stellar core are compared. Where the ISPSM fails is in predicting the detailed nuclear spectra, a task for which particle interactions (usually referred to as the "residual Hamiltonian") must be included. The residual Hamiltonian as it is used computationally consists in its simplest form of the interaction matrix elements for each pair of single particle states.

In order to compute the energy level spectrum of a nucleus using the shell model, we first construct configurations of nucleons in the ISPSM (as an example, a

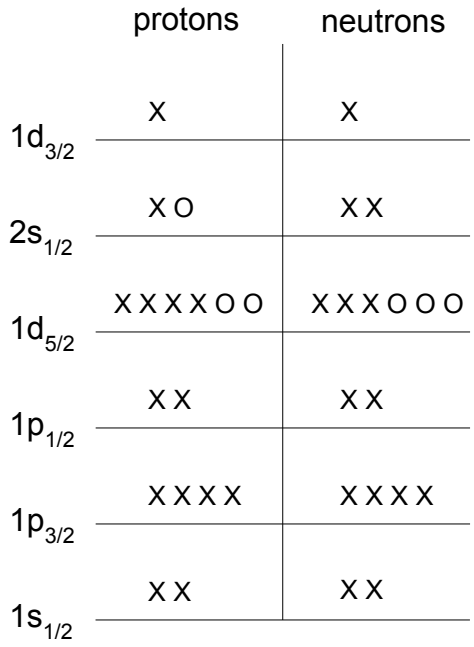

Figure 1.1: One possible single particle configuration for ^{28}Si. States that are occupied are marked with X, while holes are indicated by O. The wave functions of the particles are summed with appropriate phases to give definite values of total nuclear spin and isospin.

particular configuration is shown in Fig. 1.1), with each configuration representing a Slater determinant of the nucleons with J and T as good quantum numbers. These configurations form a basis for the nucleus which is then diagonalized in the residual Hamiltonian to obtain total nuclear wave functions and energies.

This can be a daunting computational task because the number of possible configurations – and hence the dimension of the matrix to be diagonalized – grows rapidly with A. Therefore, some simplifications must usually be employed in order to reduce the matrix size to one that can be handled on modern computers. While no one of the following simplifications must necessarily be applied in any particular calculation, I used each in the work presented in this thesis. The first approximation is to take the nucleus to consist of a "closed core" of tightly bound nucleons completely filling all of the single particle states up to some energy, with the re-

maining "valence" nucleons free to occupy higher-lying states. The core is chosen to be a doubly magic nucleus with A = Z, *e.g.* a closed ^{16}O core or a closed ^{40}Ca core. Because magic numbers of nucleons are particularly tightly bound, this approximation works well for modest nuclear excitation energies. Second, only allow the valence nucleons to occupy single particle states within the shell immediately above the core. Again, the large energy gap between shells makes this a reasonably good approximation. Finally, only allow some of the valence nucleons to occupy single particle levels above the ISPSM ground state configuration. This is the most restrictive simplification, but it still yields satisfactory results for low-lying nuclear states.

Once the residual Hamiltonian has been diagonalized in the configuration basis, we have a set of nuclear energies and wave functions on which to perform further computations.

1.2.3 Nuclear Weak Interactions

In the same sense that the electromagnetic force is mediated by the photon, the weak interaction is mediated by the $W^{\pm}$ and Z^0 bosons, with the superscripts indicating electric charge; the magnitude of the charge is one unit of elementary charge. However, there are two key differences from electromagnetic interactions. The first is that the $W^{\pm}$ and Z^0 bosons are very massive, the former weighing in at ≈ 80 GeV, and the latter ≈ 91 GeV. Any interactions with center-of-momentum energy less than the mass of the mediating particle will take place via a virtual particle. Consequently, these enormous masses cause the weak force to be short-range, as the lifetime of a virtual particle is set by Heisenberg's uncertainty principle: $\Delta E \Delta t \geq \hbar$. Secondly, the $W^{\pm}$ bosons carry electric charge and can affect the intrinsic properties of the interacting particles, changing the particles to different species with different charge and mass.

In this work I am concerned primarily with two interactions within the nucleus: one "neutral current" interaction (mediated by the Z^0 boson) and one "charged current" interaction (mediated by the $W^{\pm}$ bosons). The neutral current nuclear de-excitation interaction shown in Fig. 2.1 and discussed in chapter 2

takes place via the isospin z-projected Gamow-Teller operator: $\widehat{\overrightarrow{\sigma} T_z}$. Here $\widehat{\overrightarrow{\sigma}}$ is the quantum mechanical spin operator, and $\widehat{T_z}$ is the nuclear z-component of isospin operator. Because isospin is taken to be a good symmetry with respect to the nuclear Hamiltonian, $\widehat{T_z}$ can change the total isospin of the nucleus, but leaves the z-projection of isospin Z − N unchanged. Neglecting fundamental constants (these are included in chapter 2), the transition amplitudes between nuclear states are given by

$$\langle \Psi_f | \widehat{\overrightarrow{\sigma} T_z} | \Psi_i \rangle = \langle \Psi_f | \sum_n \widehat{\overrightarrow{\sigma_n} \tau_{zn}} | \Psi_i \rangle \tag{1.3}$$

where $|\Psi_i\rangle$ and $|\Psi_f\rangle$ are the initial and final nuclear states, the sum is over nucleons, $\overrightarrow{\sigma_n}$ is the single particle spin operator of particle n, and τ_{zn} is the single particle z-component of isospin operator. The selection rules for the final states of this operator are $\Delta J = 0, \pm 1$, with $0 \rightarrow 0$ not allowed; $\Delta T = 0, \pm 1$, with $0 \rightarrow 0$ not allowed; $\Delta T_z = 0$; Δparity $= 0$.

The charged current interaction of chapter 3, namely electron capture, is mediated by the W^+ and W^- bosons, as shown in Fig. 1.2. Electron capture has two principle operators associated with it: the Fermi lowering operator $\widehat{T_-}$ and the Gamow-Teller lowering operator $\widehat{\overrightarrow{\sigma} T_-}$. The $\widehat{T_-}$ operator is the isospin analog of the angular momentum lowering operator; it takes an initial state with z-projection of isospin T_z to a final state with z-projection of isospin $T_z - 1$. As in the neutral current case, the nuclear operators are sums over nucleons of single particle operators. The selection rules for the Fermi lowering operator are $\Delta J = 0$; $\Delta T = 0$; $\Delta T_z = -1$; Δparity $= 0$. For the GT lowering operator, they are $\Delta J = 0, \pm 1$, with $0 \rightarrow 0$ not allowed; $\Delta T = 0, \pm 1$, with $0 \rightarrow 0$ not allowed; $\Delta T_z = -1$; Δparity $= 0$.

With the matrix elements in hand, it is now simply a matter of applying Fermi's Golden Rule

$$\lambda_{if} = \frac{2\pi}{\hbar} |M_{if}|^2 \rho(E_f) \tag{1.4}$$

to obtain the transition rates, where λ_{if} is the transition rate from the initial state to the final state, M_{if} is the matrix element (including fundamental constants) connecting the two states, and $\rho(E_f)$ is the density of final states. In general, the total transition rate is found by averaging Eq. 1.4 over initial states and summing

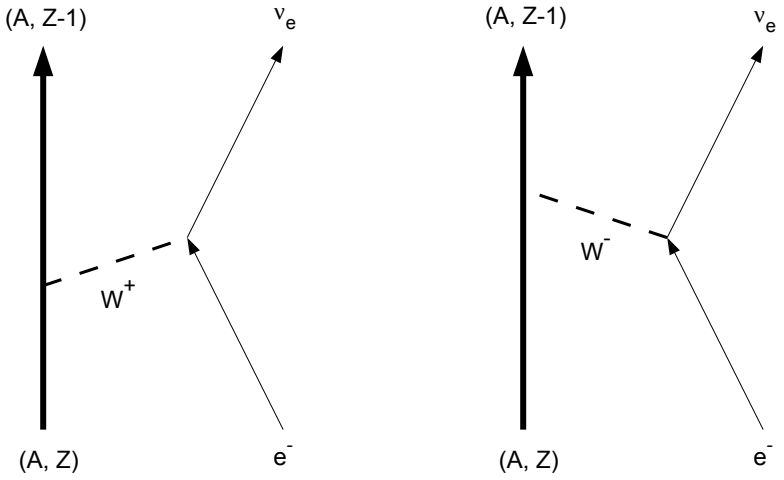

Figure 1.2: Feynman diagram showing electron capture. An incoming nucleus with mass number A and proton number Z and an incoming electron exchange a W^+ or W^- boson, resulting in an outgoing nucleus with proton number Z-1 and an outgoing electron-flavored neutrino.

or integrating over final states. For the transitions addressed in this work, this is done with thermal population of initial nuclear states, sums over final nuclear states, and phase space integrals over the momenta (or equivalently, energies) of the incoming and outgoing particles.

Chapter 2

Neutral Current De-excitation of Hot Nuclei During Stellar Collapse

2.1 Abstract

We present shell-model calculations showing that residual interaction-induced configuration mixing enhances the rate of neutral current de-excitation of thermally excited nuclei into neutrino-antineutrino pairs. Though our calculations reinforce the conclusions of previous studies that this process is the dominant source of neutrino pairs near the onset of neutrino trapping during stellar collapse, our shell-model result has the effect of increasing the energy of these pairs, possibly altering their role in entropy transport in supernovae.

2.2 Introduction

In this paper we study the role of the nucleon-nucleon interaction in the process of de-excitation of hot, excited nuclei into virtual Z^0's and neutrino-antineutrino pairs. This process is likely the dominant source of neutrino pairs in collapsing stellar cores [13, 27, 28]. The energy of the neutrinos in these pairs,

set in part by nuclear structure considerations, can be an important determinant of entropy transport in core collapse supernovae. In turn, the entropy figures prominently in the nuclear composition, neutronization history, and initial shock energy in supernova models.

The entropy per baryon in the collapsing stellar core is low and, as a result, most nucleons reside in large nuclei and there are very few free protons [10,16]. The paucity of free protons has the effect of suppressing the overall electron capture rate [16], yielding a greater electron fraction Y_e (electrons per baryon). Most pressure support within the core comes from electron degeneracy, so higher Y_e during collapse implies a larger pressure and, hence, a larger homologous core mass. The mass of this inner core determines the initial energy of the post-bounce shock: a more massive inner core yields a stronger initial shock. The strength of the shock, the mass of the core above the shock, and photo-dissociation of heavy nuclei in this outer core (all determined in part by Y_e) are important parameters in the supernova explosion process [3–9, 29–34].

In the epoch near neutrino trapping, when the core density is $\sim 10^{12}\,\mathrm{g\,cm^{-3}}$, the electron fraction is $Y_e \approx 0.32$ [29], giving an electron Fermi energy $\mu_e \approx 51.5\,\mathrm{MeV}\ (\rho_{12}\,Y_e)^{1/3} \approx 35\,\mathrm{MeV}$, where the density is scaled as $\rho_{12} \equiv \rho/10^{12}\,\mathrm{g\,cm^{-3}}$. The temperature of the core is in the neighborhood of $T \sim 1\,\mathrm{MeV}$ to $2\,\mathrm{MeV}$, so the electrons are highly degenerate. (In this paper we use natural units and set $\hbar = k_\mathrm{b} = c = 1$.) Energy emission from the core via neutrinos helps to maintain low entropy, but at a core density of $\rho_{12} \sim 1$, high energy neutrinos are trapped by neutral current coherent scattering on nuclei. However, since the cross-section for this process varies as the square of neutrino energy, low energy ($E_\nu < 10\,\mathrm{MeV}$) neutrinos may escape, carrying away entropy and possibly, depending on the process, lepton number.

There are a number of ways to produce low energy neutrinos in the core: inelastic down-scatter of neutrinos on electrons [35, 36]; electron neutrino-pair bremsstrahlung; plasmon decay, *etc.* [12, 37–44]. However, most of these processes involve either electrons losing energy or the creation of virtual electrons, both of which are suppressed by the extreme electron degeneracy; in these conditions there

simply isn't much phase space available below the Fermi level. Inelastic neutrino down-scatter on electrons involves electrons *gaining* energy and is probably the dominant source of low-energy electron neutrinos, since there is phase space above the Fermi sea for electrons to move into. But even this process is not completely unblocked, as only electrons within ΔE (where ΔE is the energy transferred from the neutrino to the electron) of the Fermi level can participate.

This leads us to explore low-energy neutrino production mechanisms that do not involve electrons. Simple neutral current neutrino-nucleon down-scattering tends to be ineffective in this regard. This is because this process is roughly conservative: the nucleon mass is large compared to the typical electron capture-generated neutrino energies, $E_\nu \sim 25\,\mathrm{MeV}$. Free nucleon neutrino-pair bremsstrahlung [45–47], a key process in neutron star cooling, is less effective here because of phase space considerations and because there are few free nucleons in the low entropy conditions that favor large nuclei during stellar collapse.

Indeed, there are analogs of these two processes for nucleons that reside in the large nuclei characterizing the neutrino trapping epoch, and these are not subject to the limitations of their free nucleon cousins. These analogs are: inelastic down-scattering of energetic neutrinos on nuclei; and neutrino pair emission from thermally-excited nuclei [11, 13, 27]. The first of these processes has a relatively large cross section, as this channel is what Ref. [13] termed an "up" transition, where the nucleus acquires energy from the neutrino, implying that nucleons transition to higher nuclear excited states, where they are relatively less Pauli blocked. These processes can have important implications for supernovae [13, 48–51].

In contrast, the second of these, the nuclear de-excitation into neutrino pairs channel shown in Fig. 2.1, is a "down" transition, subject to more nuclear Pauli blocking, and therefore possessing considerably less nuclear weak interaction strength on average than the neutrino inelastic down-scatter channel. Nevertheless, the de-excitation process has some unique features: in principle it may produce lower energy neutrinos than the down-scattering channel and, should these escape the core, entropy will be lost but electron lepton number will not be. As shown in Ref. [28], hot nuclei can also de-excite into neutrino pairs through a virtual plasmon

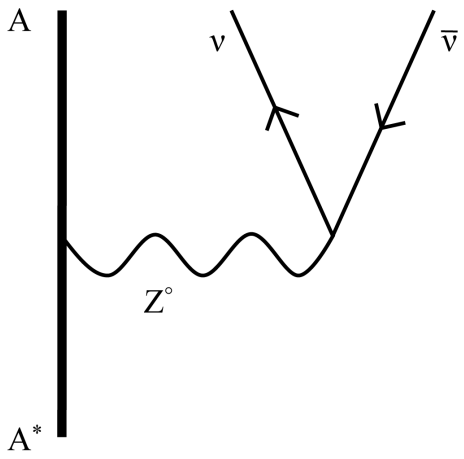

Figure 2.1: Neutral current neutrino pair emission from an excited nucleus A*.

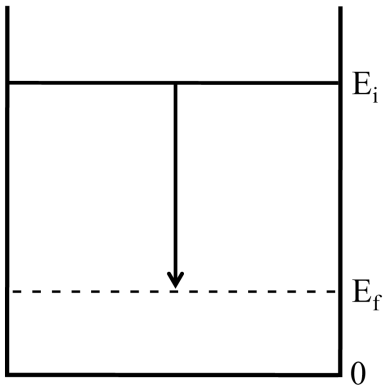

Figure 2.2: Thermally populated nuclear state with excitation energy E_i de-excites via virtual Z^0 emission to a final state with excitation energy E_f.

(photon collective mode in the plasma), and this process has been argued to lead to large enhancement factors in nuclear neutrino pair emission in the first forbidden channel. As we will show, our nuclear structure considerations also impact this channel. All of these issues depend to some extent on the nuclear physics of down transitions, and so this is where we concentrate in this work.

In Section II we discuss the nuclear and phase space aspects of de-excitation into neutrino pairs. Nuclear shell-model considerations are discussed in section III. In Section IV we discuss results, and in Section V we give conclusions.

2.3 De-Excitation Rates and Nuclear Structure

2.3.1 Large, Highly-Excited Nuclei During Core Collapse

Strong and electromagnetic interactions are fast enough that the material in stellar collapse can be in thermal and chemical equilibrium, *i.e.,* Nuclear Statistical Equilibrium (NSE). The weak interaction also is driving toward equilibrium (beta equilibrium) at the epoch of neutrino trapping, but has not yet arrived there. The pioneering work by Bethe *et al.*, Ref. [10], showed that the entropy-per-baryon in a collapsing iron core is $s \approx 1$ and, as a consequence, most all nucleons will reside in large nuclei. Minimizing the free energy for typical conditions, for example with $\rho_{12} \sim 1$ and $T = 1\,\mathrm{MeV}$ to $2\,\mathrm{MeV}$, yields a mean nuclear mass $A \sim 100$.

The mix of nuclei in NSE in these conditions is exotic. These huge nuclei will have fair neutron excess, because $Y_e < 0.4$, implying neutron-to-proton ratios $n/p > 1.5$. Moreover, because the nuclear level density is high, these nuclei will be sitting at high excitation energies. To see this we can treat the nucleons in the nucleus as a Fermi gas. Using the familiar Bethe approximation [15] for the nuclear level density, an estimate of the average nuclear excitation energy is [10]

$$\langle E \rangle \approx a\,T^2, \tag{2.1}$$

where the level density parameter is $a \approx A/8\ \mathrm{MeV}^{-1}$. For example, with $A = 100$ and $T = 2\,\mathrm{MeV}$, Eq. 2.1 implies an excitation energy $\langle E \rangle \sim 50\,\mathrm{MeV}$. The expression in Eq. 2.1 is easily understood: The number of nucleons excited above the nuclear neutron and proton Fermi levels will be $\approx a\,T$, and in thermal equilibrium each nucleon so excited will have an average excitation $\sim T$.

2.3.2 Nuclear De-Excitation Rates

Consider an excited nucleus dropping down to a lower excitation energy via virtual Z^0 emission, as depicted in Fig. 2.2. This is similar to a nuclear M1 gamma transition. The de-excitation rate [11, 13] from initial nuclear state $|i\rangle$,

with excitation energy E_i, to final nuclear state $|f\rangle$, with excitation energy E_f, is

$$\lambda_{if} \approx \frac{G_{\rm F}^2\, g_{\rm A}^2}{60\,\pi^3}\,(\Delta E)^5\,B(GT)_{if} \tag{2.2}$$

$$\approx 1.71\times 10^{-4}\,{\rm s}^{-1}\left(\frac{\Delta E}{\rm MeV}\right)^5 B(GT)_{if} \tag{2.3}$$

where $G_{\rm F}$ is the Fermi constant, $g_{\rm A}\approx 1.26$ is the axial vector coupling constant, $\Delta E = |E_i - E_f|$ (hereafter referred to as the transition energy) is the difference between the initial and final state nuclear excitation energies, and $B(GT)_{if} = |\langle f||\Sigma_k(\overrightarrow{\sigma}\ t_z)_k||i\rangle|^2/(2J_i+1)$ is the reduced transition probability associated with the axial vector operator. The matrix element connects initial nuclear state $|i\rangle$ with final nuclear state $|f\rangle$. Here $\overrightarrow{\sigma}$ is the Pauli operator and t_z is the z-component of nuclear isospin. For the nuclei we consider here, only the axial vector matrix element is significant: when we neglect the relatively small Coulomb effects, the nuclear part of the Hamiltonian commutes with isospin operators (*e.g.,* T_z), and the weak vector matrix element $|\langle f|T_z|i\rangle|^2$ is zero.

The corresponding neutrino-plus-antineutrino energy emission rate, Λ_{if}, for this transition is the product of the de-excitation rate and the transition energy. Whether or not the neutrinos carrying this energy escape from the star without scattering, thereby turning the energy emission rate into an *energy loss rate*, depends on many factors, most especially the neutrino energies.

The total energy emission rate for an excited nucleus in initial state $|i\rangle$ is the sum of the energy emission rates to all accessible final states, and can be viewed as a function of E_i,

$$\Lambda_i^{\rm tot}\,(E_i) = \sum_{f,\ E_f\le E_i} |E_f - E_i|\,\lambda_{if}. \tag{2.4}$$

The total overall energy emission rate for the entire nucleus follows on performing a population index-weighted sum over all initial states i,

$$\Lambda_{\rm tot} = \sum_i P_i\ \Lambda_i^{\rm tot} \approx \frac{1}{Z}\int_0^\infty \tilde{\rho}\,(E_i)\,e^{-E_i/T}\,\Lambda_i^{\rm tot}\,dE_i, \tag{2.5}$$

where $P_i = (2J_i+1)\exp(-E_i/T)/Z$ is the population index for state i, with J_i the spin of level i, $Z = \sum_i (2J_i+1)\exp(-E_i/T)$ is the nuclear partition

function, and $\tilde{\rho}(E_i)$ is the nuclear level density at excitation energy E_i.

For the thermodynamic conditions relevant for NSE near $\rho_{12} \sim 1$, we can get a crude estimate of $\Lambda_{\rm tot}$ by simply evaluating $\Lambda_i^{\rm tot}$ at the mean excitation energy for temperature T, *i.e.,* taking $E_i = \langle E \rangle$,

$$\Lambda_{\rm tot} \approx \Lambda_i^{\rm tot} \left(E_i = \langle E \rangle \right) . \tag{2.6}$$

The rationale for this approximation is that while the nuclear level density rises nearly exponentially with excitation energy, the Boltzmann factor in Eq. 2.5 falls exponentially with this energy, so that their product is strongly peaked at $\langle E \rangle$.

However, using this rough approximation is problematic. The level density is high near $\langle E \rangle$, and there will be many different kinds of nuclear many-body states with *e.g.,* different spins and isospins, but all with roughly this excitation energy. Therefore, choosing a single representative state is not possible.

2.4 Shell-Model Considerations

2.4.1 Approaches to the Problem

Evaluating the energy emission rates in Eq. 2.4 and Eq. 2.5 for a nucleus with nuclear mass number $A \sim 100$ at a mean excitation energy $\sim 50\,{\rm MeV}$ is clearly impractical with conventional nuclear structure techniques tailored to capture low excitation energy physics. The shear size of the problem, some two dozen particles excited above the Fermi surface in a mass ~ 100 nucleus with all of the fp-, gd-, and gh-shells in play, precludes this route.

There are two possible alternative approaches: (1) Treat the $\sim a\,T$ nucleons excited above the Fermi sea as nearly free particles within a dense environment, with appropriate phase space modifications, and then calculate the neutrino-pair bremsstrahlung rates for these; and (2) Exploit the fact that each nucleon excited above the nuclear Fermi level has only a relatively small amount of energy ($\sim T$), so that conventional shell-model treatments are efficacious, at least for nuclei with

low enough mass that the problem is tractable computationally. The first of these, by treating valence nucleons as plane waves [27], will tend to overestimate [13] the nuclear weak strength available, but has the advantage that it would go smoothly to the homogeneous matter limit when nuclei merge at high density ($\rho_{12} > 10$).

Here we will take up the second approach, in part because it has the advantage of getting a better handle on the weak nuclear strength, nuclear structure effects, and energetics. The latter is an especially critical issue since the neutrino energy emission rates scale like six powers of the transition energies. Therefore, ascertaining how *e.g.,* configuration mixing and particle-hole repulsion act is important. However, we will have to model nuclei with lower masses, generally *sd*-shell and fp-shell species, rather than the mass ~ 100 nuclei that neutrino trapping NSE conditions pick out. At best, this approach will allow us to see trends that may at some point facilitate extrapolation of these considerations to enable estimates for rates from heavier nuclei.

2.4.2 Extension to Heavy Nuclei

Even calculating the de-excitation rate from a single level in a "small" nucleus is a challenging and unusual nuclear structure problem, in part because matrix elements between highly excited states are required. We have approached this using a conventional nuclear shell model with the usual filled closed core of nucleons in low-lying single-particle states plus valence nucleons in a model space. We then employ the Lanczos iteration with an appropriate nuclear Hamiltonian to generate converged eigenstates corresponding to excitation energies from the ground state to high values.

Using the shell-model code Oxbash [52], we performed a full *sd*-shell calculation of ^{28}Si using the USDB Hamiltonian [53] (closed ^{16}O core with 12 valence nucleons in the $1d$ and $2s$ shells). We performed a full fp-shell calculation of ^{47}Ti using the GPFX1 Hamiltonian [54] (closed ^{40}Ca core with 7 valence nucleons in the $1f$ and $2p$ shells). Finally, we performed a truncated fp-shell calculation for ^{56}Fe using the GPFX1 Hamiltonian, only allowing up to 2 valence protons and up to a total of 4 valence nucleons to occupy single-particle states above the zero-order (no

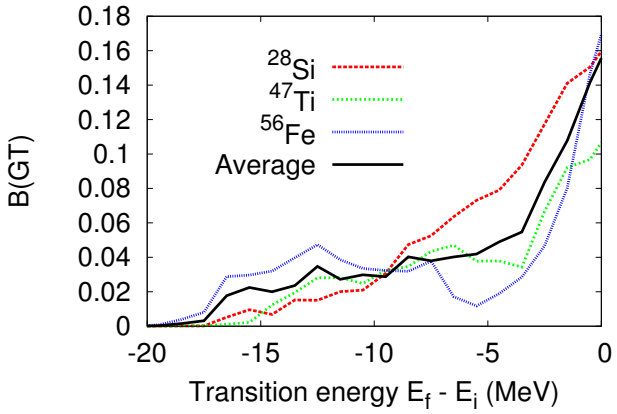

Figure 2.3: Neutrino-pair emission transition strength for ^{28}Si (averaged over 12 initial states), ^{47}Ti (2 initial states), and ^{56}Fe (3 initial states) at 27.6 MeV initial excitation shown as functions of the difference between initial excitation energy E_i and final excitation energy E_f.

residual interaction) ground state configuration. Some of the *sd* calculations were carried out with the NuShellX code [55]. With 10,000 Lanczos iterations, states up to about 40 MeV are converged to 1 keV precision.

When experimental Gamow-Teller beta-decay strengths are compared to the results obtained from calculations in the *sd* and *pf* model spaces it is observed that experimental strengths are uniformly reduced relative to theory by a factor of 0.5-0.6 [56, 57]. This "quenching" is mainly due to second-order configuration mixing induced by the short-ranged part of the tensor interaction [58, 59]. We assume that the same quenching applies to transitions from the excited states and we use a reduction factor of $r = 0.50$.

We examined transition strengths and energy loss rates over a range of excitation energies from 0 to 40 MeV in ^{28}Si and ^{56}Fe and at 23 and 27.6 MeV excitation in ^{47}Ti. The strength distributions for all three nuclei at 27.6 MeV excitation are shown in Fig. 2.3 along with the distribution obtained by averaging the strength as a function of transition energy over all three nuclei. While the details of the shapes of the strength distributions vary between nuclei, the essential feature of a central peak with a long tail out to transition energies of 15 or 20 MeV is consistent.

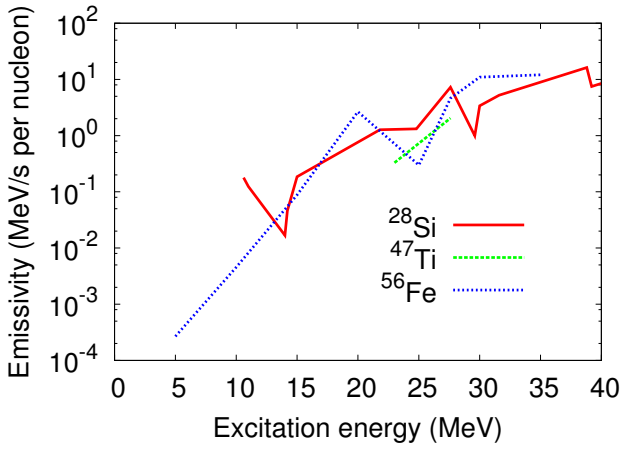

Figure 2.4: Energy loss by neutrino-pair emission shown as functions of excitation energy.

To obtain energy emission rates per nucleon as functions of excitation energy, shown in Fig. 2.4, we applied Eq. 2.4 to each nucleus, then divided by A. With an eye toward extension to large nuclei, the key observation is that the energy loss rate *per nucleon* is strongly dependent on excitation energy, but nearly independent of nucleus, despite the considerable differences in the models used for each nucleus.

To find temperature as a function of mean excitation energy and nucleus, we invert Eq. 2.1. This, along with the approximation in Eq. 2.6, gives emission rate per nucleon as a function of temperature, shown in Fig. 2.5. Also shown is the result for ^{28}Si, but with the temperature computed from excitation energy as though it had the same mass number as ^{56}Fe. As can be seen from Eq. 2.1, this amounts to scaling the temperature of ^{28}Si by a factor of $\left(\frac{28}{56}\right)^{1/2}$. This allows us to compare the ^{28}Si (our most realistic model) and ^{56}Fe (our most astrophysically relevant nucleus) results directly as functions of temperature: the comparison of the scaled results in Fig. 2.5 is equivalent to what is shown in Fig. 2.4. We use this method of temperature scaling extensively throughout this paper; it will be indicated in each case.

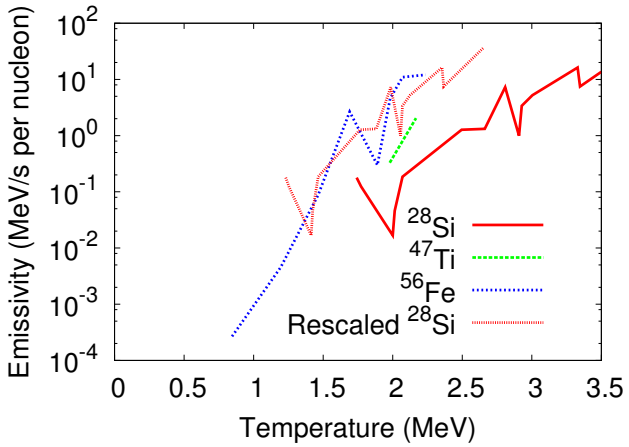

Figure 2.5: Energy loss by neutrino-pair emission for ^{28}Si, ^{47}Ti, and ^{56}Fe shown as functions of temperature. The "rescaled"line shows the ^{28}Si result with the temperature scaled by a factor of $\left(\frac{28}{56}\right)^{1/2}$, allowing the ^{28}Si and ^{56}Fe results to be compared directly at equivalent excitation energies, as in Fig. 2.4.

2.5 Results

We found that the weak strength in transitions from highly excited initial states is spread significantly in energy. The ^{28}Si results for the distribution of axial vector strength (B(GT): squared matrix element) with transition energy and the corresponding neutrino-pair energy spectrum are shown in the lower and upper panels, respectively, of Fig. 2.6. This plot shows both "up" transition strength, corresponding to positive values of $E_f - E_i$, and "down" strength with negative values of $E_f - E_i$ appropriate for de-excitation into neutrino pairs. We obtained these distributions by averaging over ten states with $J_i = 5$ near each indicated initial excitation energy; $J_i = 5$ was chosen because the *sd* shell $(2J + 1)$ state density peaks at this spin value. The distributions in the lower panel of Fig. 2.6 are plotted only up to the point where the final state eigenvalues are converged; the emission rates plotted in the upper panel are fully converged. At 20 and 30 MeV excitation, there is obviously more strength in the up than in the down channel. For a better calculation of the entire strength distribution, one should apply the Lanczos method to the Gamow-Teller distribution functions on accurate initial states. We have not implemented the GT Lanczos method in the present set of

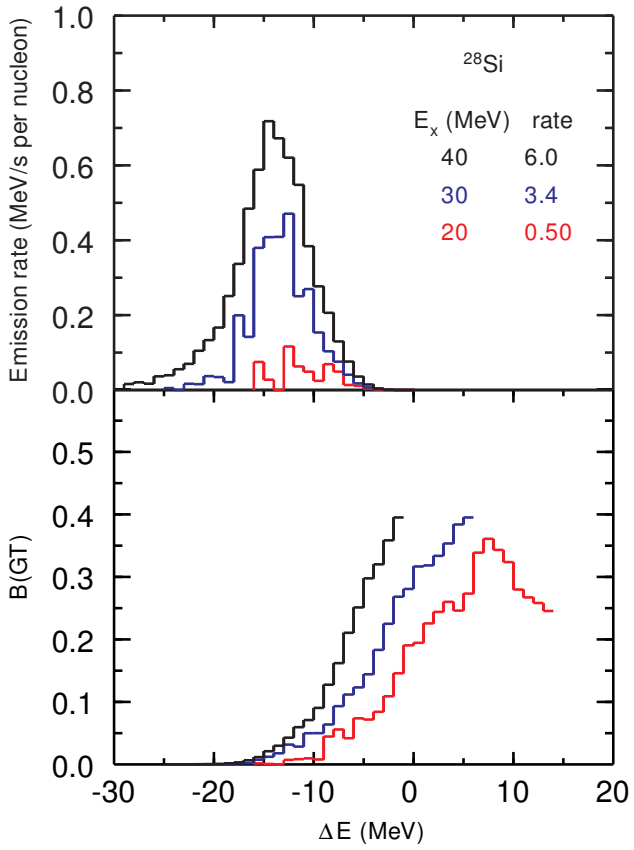

Figure 2.6: Both panels: lower line corresponds to 20 MeV excitation, middle line is 30 MeV, and upper line is 40 MeV. Bottom: Transition strengths for ^{28}Si as functions of transition energy. Top: Energy emission rates per nucleus via neutrino pairs for ^{28}Si as functions of transition energy, *i.e.*, spectra of emitted neutrino pairs.

codes, but it will not change the results of this paper for the "down" GT strength as it is computed directly from converged nuclear eigenstates.

According to Eqs. 2.3 and 2.4, the strength distribution as a function of transition energy can be multiplied by six powers of the transition energy and a constant to give the contribution of a given transition energy to the overall neutrino-pair energy emission rate, *i.e.*, the neutrino-pair energy spectrum. Although the actual strength distribution is skewed toward lower energy transitions, weighting with six powers of transition energy clearly favors larger transitions. Summing over transition energy (*e.g.,* Eq. 2.4) gives the total neutrino-pair en-

ergy emission rate per baryon. Table 2.1 shows total energy loss rates per baryon computed in this fashion for several nuclei over a range of excitation energies and temperatures (rescaled as in Fig. 2.5).

Our calculations show that the central peaks in the Fig. 2.6 strength distributions stem primarily from lateral (no spin flip) transitions. Such transitions do not change the single-particle energy of the transitioning nucleon. The wings of these strength spectra at larger transition energy come mostly from nucleon spin-flip transitions. Because configurations that result from a spin flip have a lower zero-order energy as a result of particle-hole repulsion and spin-orbit splitting, they tend to be more readily mixed down to lower excitation energy than their counterparts stemming from no-spin-flip, lateral transitions. This became abundantly clear when we computed ^{28}Si with no spin-orbit splitting in the nuclear Hamiltonian, treating the $\ell + 1/2$ and $\ell - 1/2$ single-particle states as though they have the same energy. The results of this computation are shown in Fig. 2.7, where it is readily seen that all of the strength is concentrated in a central peak, drastically reducing the rate of neutrino pair production. Since the spin-orbit splitting is due to the nuclear surface, we conclude that the Gamow-Teller down-strength is greatly enhanced when the baryons are confined to nuclei.

2.6 Discussion and Conclusions

We have found that transitions between spin-orbit partners account for the bulk of the spread to lower excitation energies (hence, larger ΔE) of the Gamow-Teller strength in this channel. That actually bodes well for any attempt to use the nuclear systematics of lighter nuclei like ^{28}Si and ^{56}Fe to effect an extrapolation of neutrino pair emission mechanisms to the higher mass nuclei of most interest in stellar collapse. This is because the spin-orbit splitting is relatively constant across nuclear mass in the range over which we are interested [60]. Particle-hole repulsion probably plays a lesser role than spin-orbit splitting in pushing strength to larger ΔE. Interestingly, the particle-hole repulsion we find in our shell-model calculations may have a direct analog in the bulk matter renormalization of the

Table 2.1: Energy loss rate (MeV/s/baryon) for various nuclei as functions of excitation energy (MeV) and the corresponding (rescaled to A=56) temperature (MeV). The unstarred rates were computed by averaging over several (5 to 14) initial states at the indicated excitation energy; starred rates were computed from 1 or 2 states. The angular momenta of all initial states are indicated. The entry ^{28}Si (no SO) was computed by neglecting spin-orbit splitting in the nuclear Hamiltonian.

Nucleus	J_i	Excitation	Rate	T (A=56)
^{28}Si	1-4	10.8	0.30	1.2
	0, 2-5	14.0	0.02	1.4
	0-5	15.0	0.22	1.5
	5	20	0.50	1.7
	0-5	20.0	0.50	1.7
	0, 2-5	21.9	1.1	1.8
	5	25	1.8	1.9
	1-5	25.0	1.8	1.9
	0-5	27.6	3.6	2.0
	5	30	3.4	2.1
	0-3, 5	30.0	3.3	2.1
	1-5	31.5	4.0	2.1
	5	35	4.5	2.2
	5	40	6.0	2.4
	0-5	40.0	8.6	2.4
^{28}Si (no SO)	5	30	0.21	2.1
^{29}Si	11/2	30	4.6	2.1
^{28}P	5	30	9.7	2.1
^{47}Ti	3/2	23.0	0.33*	1.8
	3/2, 5/2	27.6	2.0*	2.0
^{56}Fe	2	10.0	0.01*	1.2
	0	15.0	0.09*	1.5
	1	20.0	2.7*	1.7
	2	25.0	0.30*	1.9
	0, 1	27.6	4.6	2.0
	0	30.0	10.9*	2.1
	4	35.0	12.1*	2.2

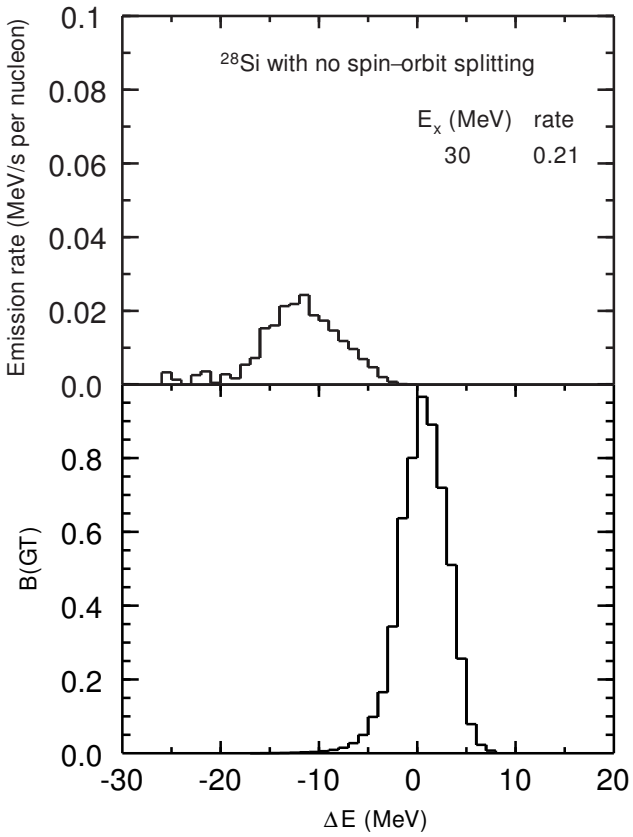

Figure 2.7: ^{28}Si strength and neutrino pair spectrum at 30 MeV excitation computed with spin-orbit splitting in the nuclear Hamiltonian set to zero. The strong central peak, lack of wings, and concomitant drastic reduction in neutrino production confirm the role of spin-orbit splitting and spin-flip transitions in producing the high rates computed in our more realistic models.

energetics of weak interaction processes as found in Ref. [61].

There are three obvious effects of skewing the strength distributions to higher transition energy ΔE. These follow from the simple fact that the neutrino-pair energy emission rate derived from the strength function is weighted by six powers of ΔE. First, more strength at higher ΔE generally means faster neutrino-pair emission rates. In turn, this means more energy will be pumped into neutrino pairs by this process. Second, the neutrinos and antineutrinos produced by this process will have higher energies on average. This brings up an obvious question: will the neutrino pair energies now be so high ($> 10\,\mathrm{MeV}$) that they are more readily trapped? Third, more configurations in play and more configuration mixing at higher excitation energy will make the transition strength and the neutrino-pair emission rate more sensitive to temperature.

We found that at expected typical supernova core temperatures the transition energies we computed are substantially greater than those found in previous work. Fig. 2.8 shows the transition strength and emission spectrum for ^{56}Fe at a temperature of 2 MeV computed using a technique very similar to the independent single particle calculation in Fuller & Meyer (1991) [13]. It clearly shows a peak in the emission spectrum at -7 to -8 MeV, which is about half the energy of the peak in our results (Fig. 2.6). These figures show only allowed strength. Of course, at substantially higher temperature, *e.g.*, $T = 5$ MeV, forbidden channel de-excitations will contribute significantly . However, typical conditions expected in realistic stellar collapse will likely not suggest temperatures this high. Moreover, the cooling engendered in part by the neutrino pair emission process discussed here will also mitigate against high temperatures.

Higher temperatures and higher excitation energies bring up an issue which is unresolved in our work. When nucleons are promoted into the next-higher oscillator level, how is the Gamow-Teller strength affected? For example, for ^{28}Si the actual level density just above roughly 10 MeV excitation will start to be dominated by one-nucleon excitations into and out of the *sd* shell (negative-parity states). This level density is shown for both positive- and negative-parity states in Fig. 2.9. The Gamow-Teller down-strength for negative-parity states will be

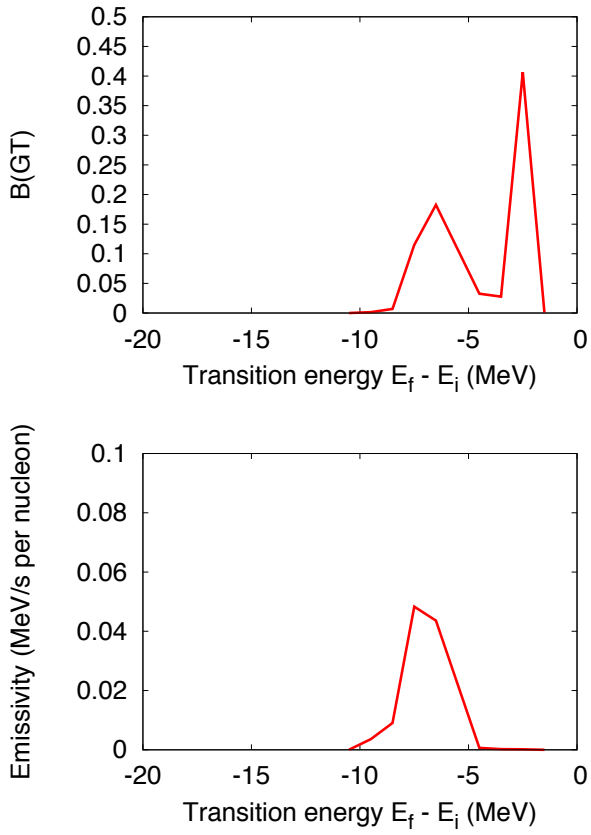

Figure 2.8: ^{56}Fe at $T = 2$ MeV computed using an independent single particle model similar to that used in Fuller & Meyer (1991) [13]. Top: Transition strength. Bottom: Emission spectrum.

relatively reduced since they must transition to negative-parity final states, and there is a paucity of these states relative to positive-parity states at low excitation.

Starting at 20 MeV excitation, more positive-parity states can be made from two nucleons excited into and out of the *sd* shell. Does this result in a lower overall amount of strength? Or is this loss of strength compensated by more transitions between spin-orbit partners in the higher energy shell? In general, it may seem reasonable that the higher the temperature and excitation energy, the "looser" the nucleus and the more transitions are unblocked [16]. However, this trend could be thwarted by the actual behavior of the level density in the shell model. Certainly, model space truncation could contribute to this if, for example, not all spin-flip transition channels in the higher oscillator level are included in the calculation. This issue may or may not complicate extrapolation of our trends in weak strength energy distributions to higher mass nuclei and requires further investigation.

The next step will be to understand how more realistic level densities affect the Gamow-Teller distribution. Explorations along these lines could be based on a statistical-type model that takes into account level density and orbital occupation numbers as a function of excitation energy. Such a model should be able to reproduce the exact results we obtain for truncated sets of single-particle states (e.g. three for the *sd* shell and four for the *pf* shell). In particular, it should reproduce the strong dependence on the spin-orbit splitting that we find. For the sake of this paper, it is sufficient to note that up to excitations of $\sim$35 MeV, our computed density of states follows a roughly exponential trend; within the *sd* shell we are in a regime where relative to lower energies, we are not missing states at or below the initial excitation energy. However, as mentioned previously, the actual level density above 10 MeV is dominated by excitations into and out of the *sd* shell.

Fig. 2.10 shows a comparison between our shell-model calculations of the neutrino-pair energy emission rate per baryon for ^{28}Si as a function of (rescaled) temperature, other estimates for this rate in ^{56}Fe as a function of temperature, the neutrino pair emission rate for electron bremsstrahlung as a function of temperature assuming a density $\rho_{12} = 1$ [12], and the neutrino pair emission rate for

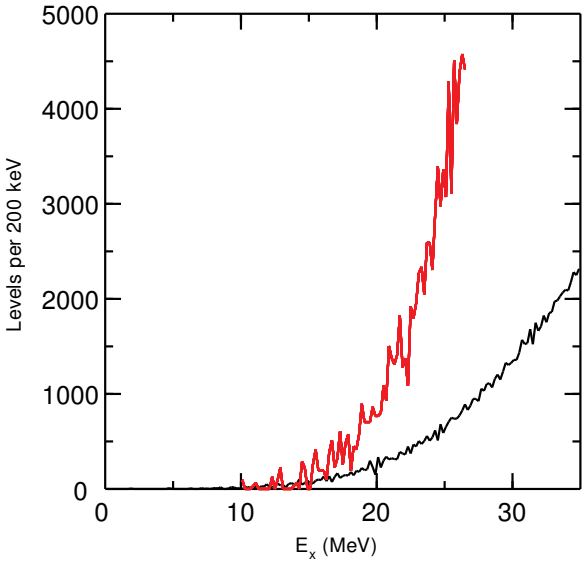

Figure 2.9: Computed density of states as a function of excitation energy for ^{28}Si. Upper line: negative-parity states. Lower line: positive-parity states.

nucleon bremsstrahlung in nuclear matter as a function of temperature [62]. We include the nucleon bremsstrahlung result to show that collectivity within the nucleus enhances the emission rate relative to bulk nuclear matter. We found that in the temperature regime of interest, our calculations can yield neutrino-pair energy emission rates that equal or exceed earlier estimates [13, 27] at all temperatures. As a general rule, our estimates of these rates are approximately three orders of magnitude faster than neutrino pair production from electron bremsstrahlung.

Clearly, de-excitation of nuclei is the dominant contributor of relatively low-energy neutrino pairs under these conditions. Moreover, the rates presented here are lower bounds on the actual neutrino-pair production rates, particularly at temperatures between 1 and 1.5 MeV. The small number of nucleons in a ^{28}Si nucleus gives a relatively low density of states at the temperatures of interest. As a consequence, there are few lower-lying states to transition to, which reduces the total transition rate. Indeed, the apparent decrease in emission rate of ^{28}Si at a (rescaled) temperature of 1.4 MeV is a consequence of the simple fact that no states near 14 MeV excitation have transitions with energies greater than those available to states near 10.8 MeV transition.

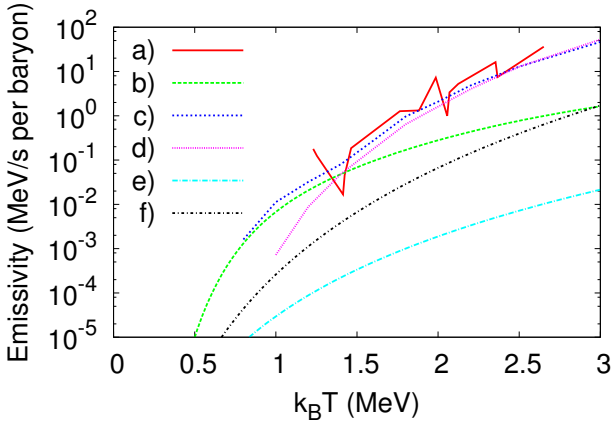

Figure 2.10: Energy per baryon emitted in neutrino pairs as a function of temperature. a) ^{28}Si as computed in this paper. b) ^{56}Fe from Fuller & Meyer independent single-particle shell-model calculation [13]. c) ^{56}Fe from Fuller & Meyer analytic approximation [13]. d) ^{56}Fe from Kolb & Mazurek [27]. e) Electron bremsstrahlung into neutrino pairs for $\rho_{12} = 1$ from Dicus et al [12]. f) Nucleon bremsstrahlung into neutrino pairs at nuclear matter density from Friman & Maxwell [62].

If it turns out that the neutrinos produced by pair de-excitation have low enough energies to escape the pre-supernova star, then this process likely acts as a thermostat for the collapsing core. In this limit, as the core heated up, more neutrino pairs would be produced and escape, carrying away entropy, and perhaps keeping the core temperature near $T = 1\,\mathrm{MeV}$ to $1.5\,\mathrm{MeV}$.

However, our calculations may be suggesting that the neutrino pairs produced by de-excitation at higher temperature are so energetic that they do not escape. Though the thermostat effect will be disabled in this case, lower to intermediate energy neutrino phase space will be filled more quickly by this process, and the core will approach beta equilibrium sooner. This effect would tend to block electron capture and neutronization sooner also, but against this neutrino-nucleus and neutrino-electron down scattering will tend to heat the system, adding entropy, implying faster electron capture through more free protons and nuclear thermal unblocking [16] and, therefore, a lower Y_e, a smaller homologous core, and a concomitantly lower initial bounce shock energy.

The issue of higher energy neutrino-pairs is complicated further when considering the effects of dynamics and flavor. The energy is shared between a neutrino

and an anti-neutrino, and the energy is small compared to the mass of the nucleus. As a consequence, the energy can be shared unequally between the two neutrinos, with the nucleus absorbing whatever momentum is needed to satisfy conservation. So a low-energy partner to a high-energy neutrino could escape. Furthermore, this process is flavor blind: it produces neutrinos of all flavors at equal rates. Because high energy neutrinos within the collapsing core are produced primarily from electron capture, there is plenty of available phase space for nuclear de-excitation to produce a high energy electron anti-neutrino or a high energy neutrino or anti-neutrino of mu or tau flavor with a low energy partner that easily escapes. The resultant asymmetry between electron flavored neutrinos and anti-neutrinos could impact lepton number within the core, as it is more likely to produce a high energy electron anti-neutrino with a low energy partner than the other way around.

Another effect of the larger ΔE values suggested by our shell-model calculations may be an enhancement in the plasmon-mediated neutrino-pair nuclear de-excitation process pointed out by Horowitz in Ref. [28]. The matrix element for the first forbidden vector channel considered in Ref. [28] is $\propto \langle f|q \cdot T_z|i\rangle$, where $q \sim \Delta E$ is the momentum transfer. This first forbidden channel is in general cut down by a geometric factor, $(qR)^2 \sim 1/16$, which is the square of the ratio of the nuclear radius R to the inverse momentum transfer. Our larger values of ΔE should give a smaller reduction, increasing the overall rate of nuclear de-excitation into pairs.

Though our shell-model calculations are only a beginning, they do suggest that nuclear de-excitation into neutrino pairs is likely the dominant source of low to intermediate energy neutrino pairs in stellar collapse. Our calculations suggest a spin-orbit splitting-induced increase in the rate of this process and a steepening of the temperature dependence of this rate. These calculations also suggest, however, that the neutrinos produced in this process are more energetic and may be trapped. Only inclusion in a full core collapse neutrino transport simulation could reveal what role this process plays in core collapse supernova explosions.

2.7 Acknowledgments

This work was supported in part by NSF grant PHY-09-70064 at UCSD and NSF grant PHY-1068217 at MSU. We would also like to acknowledge support from the LANL Topical Collaboration and UCOP, and support of the Michigan State University High Performance Computing Center and the Institute for Cyber-Enabled Research. We would like to thank J. Carlson, J. Cherry, and S. Reddy for helpful discussions, and A. Y. Shih for assistance in creating Figs. 2.1 & 2.2.

Chapter 2, in full, is a reprint (with the exception of references, which have been moved to the end of this thesis) of material previously published as G. Wendell Misch, B. Alex Brown, and George M. Fuller, "Neutrino-pair Emission from Hot Nuclei During Stellar Collapse", *Physical Review C* **88** 015807 (2013), 1301.7042. I was the primary investigator and author of this paper.

Chapter 3

Modification of the Brink-Axel Hypothesis for High Temperature Nuclear Weak Interactions

3.1 Abstract

We present shell model calculations of electron capture strength distributions in A=28 nuclei and computations of the capture rates in supernova core conditions. We find that in these nuclei the Brink-Axel hypothesis for the distribution of Gamow-Teller strength fails at low and moderate initial excitation energy, but may be a valid tool at high excitation. The redistribution of GT strength at high initial excitation may affect capture rates during collapse. If these trends which we have found in lighter nuclei also apply for the heavier nuclei which provide the principal channels for neutronization during stellar collapse, then there could be two implications for supernova core electron capture physics. First, a modified Brink-Axel hypothesis could be a valid approximation for use in collapse codes. Second, the electron capture strength may be moved down significantly in transition energy, which would likely have the effect of increasing the overall electron capture rate during stellar collapse.

3.2 Introduction

The Brink-Axel hypothesis posits that the electromagnetic giant dipole resonance in nuclei resides at the same relative energy from excited states as it does from the ground state [63,64]. That is, if a given nucleus in its ground state has the resonance at 10 MeV, then that same nucleus in an excited state would have that resonance at 10 MeV above the excited level, and indeed experiment bears this out. In this paper we examine electron capture strength on nuclei with high initial excitation energy and its effect on the electron capture rate, with a particular emphasis on adapting the Brink-Axel hypothesis for use in this channel.

Neutronization of the collapsing core through electron capture is pivotally important in the supernova problem, as electrons provide pressure support within the core. During infall, the mass of the homologous inner core (that portion which collapses subsonically) is set by the electron-to-baryon ratio Y_e. This mass, which acts as a sort of piston at core bounce, sets the initial post-bounce shock energy. Moreover, Y_e figures into the nuclear composition of the outer core, which dissipates much of the shock energy through photodissociation of its nuclei and affects neutrino transport through coherent interaction with nuclei [3–9, 29–34].

During supernova core collapse, the density is very high, starting at around 10^{10} g/cm^3 at the onset of collapse and proceeding to $>10^{14}$ g/cm^3 at bounce. The temperature is very high at $\sim$1-2 MeV, but the entropy per baryon is extremely low at $\approx$1 unit of Boltzmann's constant per baryon [10]. Although electrons are most readily captured onto free protons, the low entropy favors large nuclei which are then in turn the principal sites for electron capture [10,16,29]. The core is initially cooled during collapse by neutrino emission [11–14], so the entropy remains low. Furthermore, the high temperature puts these nuclei into extremely highly excited states. Using the Bethe approximation for nuclear excitation energy [15]

$$E = a(k_B T)^2 \tag{3.1}$$

where a $\approx \frac{A}{8}$ MeV^{-1} is the level density parameter, and a typical nuclear mass of $\sim$120, we find the average excitation energy to be between 15 and 60 MeV. Finally, as the collapse progresses, the core electron fraction tends toward $Y_e \approx 0.32$, which

yields extremely neutron rich nuclei. In order to understand neutronization during core collapse, we must therefore consider the capture of electrons onto large, highly excited, and eventually neutron rich nuclei.

Large, highly excited, neutron rich nuclei are, unfortunately, problematic to understand both experimentally and theoretically. Experimental data on these nuclei is sparse [65], and while large nuclei certainly exist in abundance, there are as of yet no experimental means by which to put them into high energy states without utterly destroying them. The (n,p), (p,n), (^{3}He,t), (d,^{2}He), and similar charge exchange channels give information on the Gamow-Teller structure [66–68], but these experiments can only probe nuclei in the ground state, whereas low entropy, high temperature environments favor much higher excitations. The Extreme Light Infrastructure may eventually be able to provide some insight into the structure and behavior of highly excited nuclei through the use of multiple MeV laser light, but it is not yet in operation [69]. Of course, even when high energy states become readily attainable, we still face the problem that nuclei of the appropriate neutron richness are completely unstable in the laboratory; it is the high density and low entropy of the supernova core that allows them to exist in that environment.

From the theoretical direction, we should look for trends in the Gamow-Teller electron capture strength distribution, as the Brink-Axel hypothesis has had experimental success in the electromagnetic channel. Fuller, Fowler, and Newman [23–26] (hereafter FFNI, FFNII, FFNIII, and FFNIV, respectively, for those specific works, and FFN for the body of work as a whole) previously adapted the Brink-Axel hypothesis for use in the Gamow-Teller charged current channel (we will call this and similar techniques the GT Brink-Axel hypothesis to distinguish it from the experimentally verified electromagnetic phenomenon). This approach and modifications thereof have since been widely used to compute weak rates. Variations include essentially copying the FFN approach [70], using a broad GT resonance that is the same for all excited states [71, 72], computing in detail only the lowest few states in the parent and/or daughter nuclei and employing the GT Brink-Axel hypothesis to treat the bulk of the strength at high excitations or neglecting highly excited states entirely [17, 73–80], and using thermal averaging

techniques [81, 82]. Recently, electron capture rates have been tabulated using combinations of these approaches over a wide range of nuclear masses and stellar conditions [83].

However, some authors have observed the breakdown of the GT Brink-Axel hypothesis even at modest excitation energies [84–86]. Thus, whenever it is computationally feasible, we should avoid use of the GT Brink-Axel hypothesis. Oda et al [87] performed full sd shell model computations of the first 100 excited states in each sd shell nucleus, while others have taken to the random phase approximation to examine heavier nuclei [88, 89]. But the Oda et al approach of neglecting states higher than the 100^{th} excitation may miss some important features of higher-lying states, and while RPA does well at determining the overall strength distribution, it is unable to accurately reproduce the detailed distributions to which electron capture rates are sensitive. We are therefore well served by scrutinizing detailed strength distributions up to very high initial excitation to learn in what ways the distribution evolves. We will show that at least in the sd shell, a modified form of the GT Brink-Axel hypothesis derived from large scale shell model calculations can be both computationally tractable and capture features of the strength distribution at low and high excitation with consequences for core collapse.

Computationally, large nuclei are difficult to study simply because of the large number of nucleons involved; the sheer combinatorics of so many nucleons rapidly drives up the computational requirements. This difficulty is usually circumvented by holding most of the nucleons fixed and only allowing a few to occupy single particle states above the lowest energy. While this approach works reasonably well for the lowest-lying nuclear states, it's efficacy quickly breaks down at higher energies (higher nuclear energies imply more nucleons above the lowest single particle energies) and when the model has too few single particle states, *i.e.* is restricted, allowing too few basis states to yield a realistic set of total nuclear eigenstates.

Because of these computational obstacles and the fact that we want to understand the GT structure of *very* highly excited nuclei, we are relegated in this work to studying relatively light nuclei. The biggest drawback of this approach

is that although light nuclei are abundant prior to the onset of collapse, they are disfavored during infall. In our favor, reference [14] found that in some respects, heavy nuclei and light nuclei exhibit similar weak transition characteristics. In any case, light nuclei are at present the only option for computing highly excited states, and through them we will ideally learn something that will shed light on the behavior of all nuclei, including heavier, more neutron rich species.

In section 3.3, we provide a brief overview of the nuclear shell model and GT transitions, as it will be convenient in later sections to have that picture in mind. Section 3.4 outlines the historical approach to the problem at hand and discusses its weaknesses. The results of our electron capture strength computations are in section 3.5, and using those results, we show a calculation of electron capture rate in section 3.6. We give discussion and conclusions in section 3.7.

3.3 Nuclear Shell Model and GT Transitions

In the shell model, individual nucleons are considered to occupy non-interacting single-particle states, with the sets of occupied states (configurations) having good spin J and isospin T. These configurations form a basis for the nucleus, eigenstates of which are constructed by diagonalizing the residual nucleon-nucleon Hamiltonian in the configuration basis, thus mixing many configurations into a single nuclear state:

$$|\Psi_{J,T}\rangle_i = \sum_k A_{ik} |C_{kJ,T}\rangle \tag{3.2}$$

where $|\Psi_{J,T}\rangle_i$ is nuclear eigenstate i with spin J and isospin T, the A_{ik} are complex amplitudes, and $|C_{kJ,T}\rangle$ is the kth configurations with spin J and isospin T.

One-body nuclear transitions – such as the Gamow-Teller transition – consist of a single nucleon changing its single particle state. There are three qualitatively different single particle GT transitions: spin flip transitions (from an $l + \frac{1}{2}$ state to an $l - \frac{1}{2}$ state), back spin flip transitions (from $l - \frac{1}{2}$ to $l + \frac{1}{2}$), and lateral transitions (no change in total angular momentum). Respectively, these represent a net gain, loss, and no change in single particle energy. If any other nuclear state has as one of its components a configuration resulting from a single particle

transition, then the nucleus can transition to that final state. The strength of the transition from an initial nuclear state $|i\rangle$ to a final state $|f\rangle$ is given by

$$|\langle f| \sum_k \widehat{o_k} |i\rangle|^2 \tag{3.3}$$

where $\widehat{o}$ is the single body operator and the sum is over nucleons. Throughout this paper, "GT strength" will refer to the reduced nuclear transition probability $\mathrm{B(GT)}_{if}$, given by

$$\frac{|\langle f||\Sigma_k(\vec{\sigma}\tau_-)_k||i\rangle|^2}{2J_i+1} \tag{3.4}$$

where $\vec{\sigma}\tau_-$ is the one-body Gamow-Teller lowering operator and the sum is over nucleons.

3.4 Previous Adaptation of GT Brink-Axel Hypothesis

FFNII [24] approached the problem of GT transition strength distributions by using experimental values of the strength where known, supplementing that with estimated allowed and forbidden strength to known states in the daughter nucleus, and placing the remainder of the GT strength computed from a zero-order shell model into a single resonance, the energy of which was also computed using a zero-order shell model. Using two simple assumptions, FFNII took the strength and relative energy of the resonance to be the same for all excited states as it is for the ground state. First, assume that the individual nucleons are distributed among the single particle states in a way that is *on average* independent of nuclear excitation energy. Second, assume that the transition energy of the GT resonance is principally due to a single nucleon undergoing a spin flip, and thus is similar in excited states to that of the ground state. To the extent that these approximations are valid, they are extremely useful, as the partition function becomes algebraically irrelevant in determining the resonant electron capture rate. From FFNII, the total electron capture rate through resonant transitions is given by

$$\Lambda^{res} = \sum_i P_i \lambda_i^{res} \tag{3.5}$$

where P_i is the probability that the nucleus is in state $|i\rangle$ (given by the product of the degeneracy and the Boltzmann factor, divided by the partition function) and λ_{if}^{res} is the resonant transition rate from state $|i\rangle$ to state $|f\rangle$, itself a function of nuclear structure and electron distribution in the supernova core. But under the assumption that the GT resonances are the same–irrespective of nuclear excitation energy–all of the λ_i^{res} are identical; we shall call them λ^{res}. We now have

$$\begin{aligned} \Lambda^{res} &= \sum_i P_i \lambda^{res} \\ &= \lambda^{res} \sum_i P_i \\ &= \lambda^{res} \end{aligned} \tag{3.6}$$

So, the total resonant transition rate is simply the resonant transition rate of any single state, which we take to be the ground state. Of course, highly excited states in the parent would be in the GT resonances of lower energy states in the daughter, leading to "back-resonant" transitions. Accounting for the fact that the P_i will not sum to unity for back-resonant transitions and otherwise treating them identically to resonant transitions, we eventually arrive at

$$\Lambda^{backres} = \lambda^{backres} \frac{G^d}{G^p} e^{\frac{-R}{kT}} \tag{3.7}$$

where G^p (G^d) is the partition function of the parent (daughter) nucleus and R is the characteristic transition energy of the GT resonance from the daughter nucleus to the parent. Finally, Fermi transitions are handled in an identical manner to the GT transitions, and the rates are summed along with the rates from known and estimated transitions to get the total capture rate.

A priori, we might expect the GT Brink-Axel hypothesis to fail. If we keep the assumption that single particles are distributed roughly independently of nuclear excitation energy, we should be unsurprised if the GT resonance moves dramatically or is redistributed in transition energy, since at sufficiently high initial excitation, there will be strength for the daughter nucleus to be at *many* energies relative to the parent, without any particular single particle transition dominating the strength. Since by assumption the single particles in all of these daughter

states are also arranged similarly, we would rather expect the GT strength to be broadly distributed in transition energy. The question, then, is in what way does the hypothesis fail? Do strength distributions evolve in some characteristic way as initial excitation energy increases, or must we abandon the hypothesis completely and replace it with a thermal mean strength distribution?

3.5 GT Strength Computations

Using the shell model code Oxbash [52], we performed shell model calculations of $A = 28$ nuclei using a closed ^{16}O core and 12 valence nucleons in the sd shell. Although $A = 28$ is unrealistically light for the supernova core environment, we chose to use it because it provides a good balance of complexity and computability; that is, we have many valence nucleons and holes (implying many single particle configurations), but there are few enough configurations that we can compute nuclear eigenstates in a reasonable time.

The sd shell consists of the single particle sates $1d_{5/2}$, $2s_{1/2}$, and $1d_{3/2}$. In these computations, we used the USDB Hamiltonian [53], with single particle energies -3.9257, -3.2079, and 2.1117 MeV, respectively. In the GT interaction, nucleons can transition from $2s_{1/2}$ to $2s_{1/2}$, and from either d sub-orbital to either d sub-orbital.

In order to make an apples-to-apples comparison with the FFN results, we neglect quenching throughout this work.

3.5.1 ^{28}Si

We first examined ^{28}Si. Although this nucleus is neutron poor by supernova collapse standards, it has the most single particle configurations among sd nuclei and therefore computationally is the most realistic. We found that the GT Brink-Axel hypothesis as originally formulated does not obtain in that the strength distributions of excited states bear no resemblance to the ground state. However, at initial excitation energies greater than 12 or 16 MeV, the GT strength distribution is almost independent of initial state energy, although its shape does depend

on the initial isospin. Fig. 3.1 shows the strength as a function of excitation energy and nuclear transition energy (that is, the total energy input required to make the transition, including the change in nuclear mass).

Although initial isospin evidently plays a role in the strength distribution, we found that the strength does not depend strongly on initial spin. Fig. 3.2 shows the strengths for a representative selection of spins with initial isospin $T_i = 0$. Evidently, we can safely neglect spin in our analyses.

The shapes of the strength distributions can be partially understood by decomposing them into contributions from final states with specific isospin (Fig. 3.3); the strength distribution is strongly dependent on the final isospin. It can be clearly seen that the small peak in the total strength distribution at $\Delta E \approx 17$ MeV for states with $T_i = 2$ is due to transitions to final states with $T_f = 3$.

Finally, we sought an understanding of the similarity of the strength distributions in the high excitation energy regime. To this end, we examined single particle distribution as a function of nuclear excitation energy. Fig. 3.4 shows the average single particle state occupation as a function of excitation energy for T= 0 states in ^{28}Si. The most salient feature is that the 1d state occupations have a linear dependence on nuclear excitation with slopes of roughly 1 particle per 12 MeV (which is approximately the spin-orbit splitting energy + particle-hole repulsion energy in this sub-shell), while the $2s_{1/2}$ occupation is independent of excitation; this is in contrast to reference [24], which assumed that the average occupations of all single particle states were independent of nuclear excitation energy. While Fig. 3.4 shows only T= 0 states, the trends are consistent for all isospins, with the exception that the intercept of the $1d_{3/2}$ ($1d_{5/2}$) occupation gradually shifts by -1 (1) particle as T goes from 0 to 3, and shifts an additional -1 (1) particle as T goes from 3 to 4.

Since we did the computations in this paper with isospin as a good quantum number, we can take the single particle occupations in Fig. 3.4 to be split proportionately between the valence protons and neutrons. In the case of ^{28}Si, then, the proton and neutron single particle occupation numbers are each 1/2 the total occupation. This implies that the 1 particle per 12 MeV slope in fig. 3.4

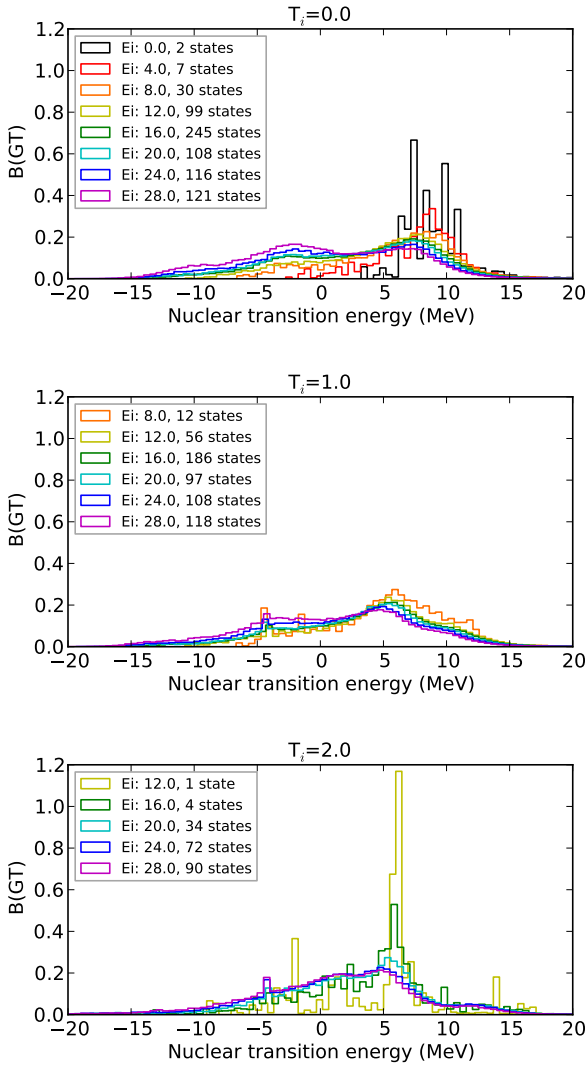

Figure 3.1: Gamow-Teller strength distribution as a function of initial isospin T and excitation energy. Initial state energies are binned in 4 MeV increments. The strength distribution has an apperent dependence on initial isospin, though the dependence on excitation energy becomes small at high excitation.

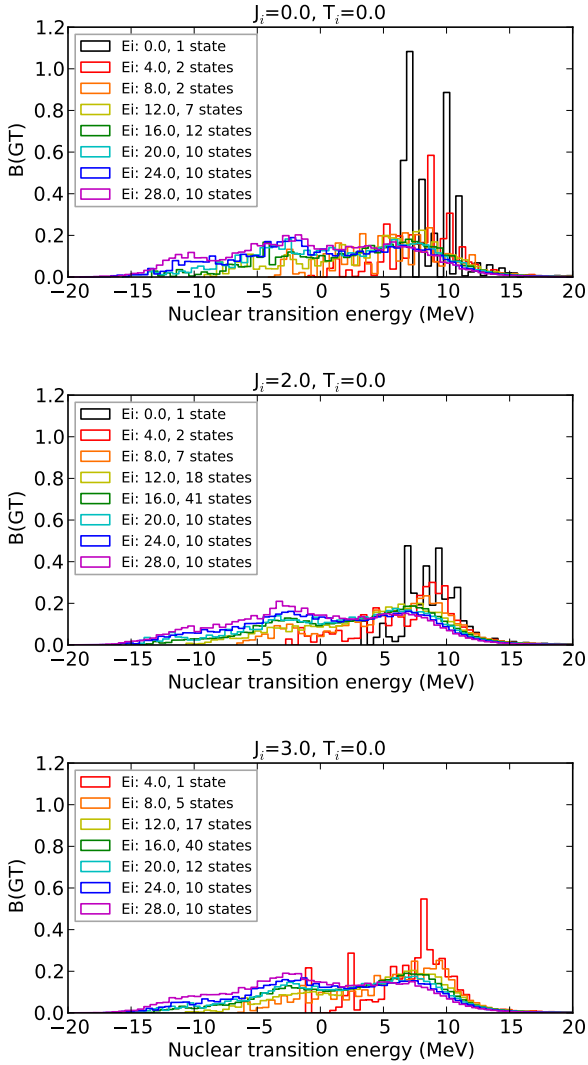

Figure 3.2: GT strength distributions as a function of initial spin J_i and excitation energy with initial isospin $T_i = 0$. It is readily seen that the strength distribution is not strongly dependent on J_i. We saw this trend in all nuclei we studied.

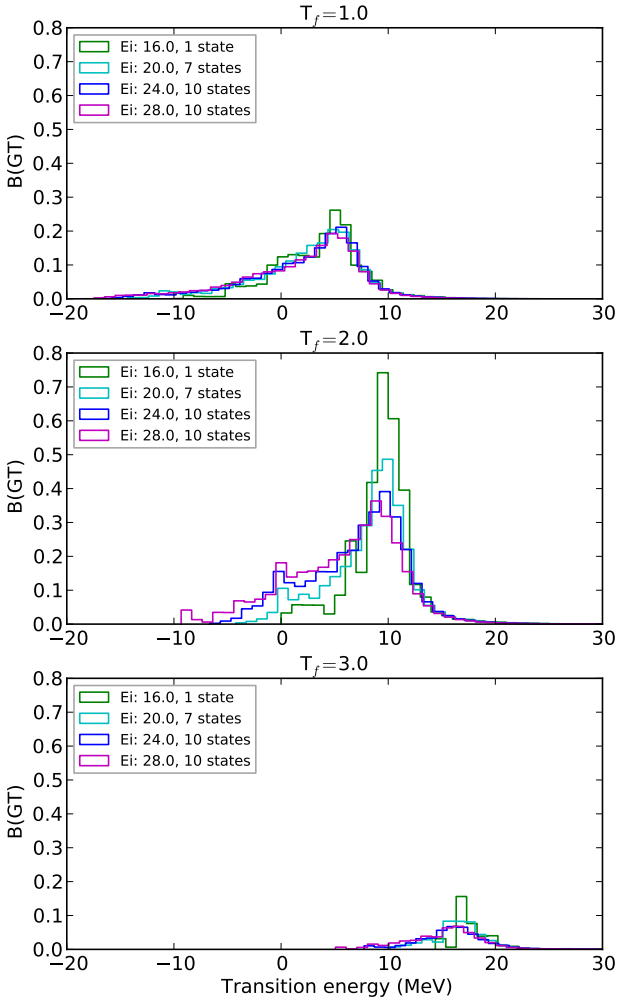

Figure 3.3: Strength distribution for ^{28}Si with initial spin $J_i = 4$, initial isospin $T_i = 2$ as a function of final state isospin. Comparison with Fig. 3.1 shows that certain features of the total strength distribution are a consequence of the available final state isospins.

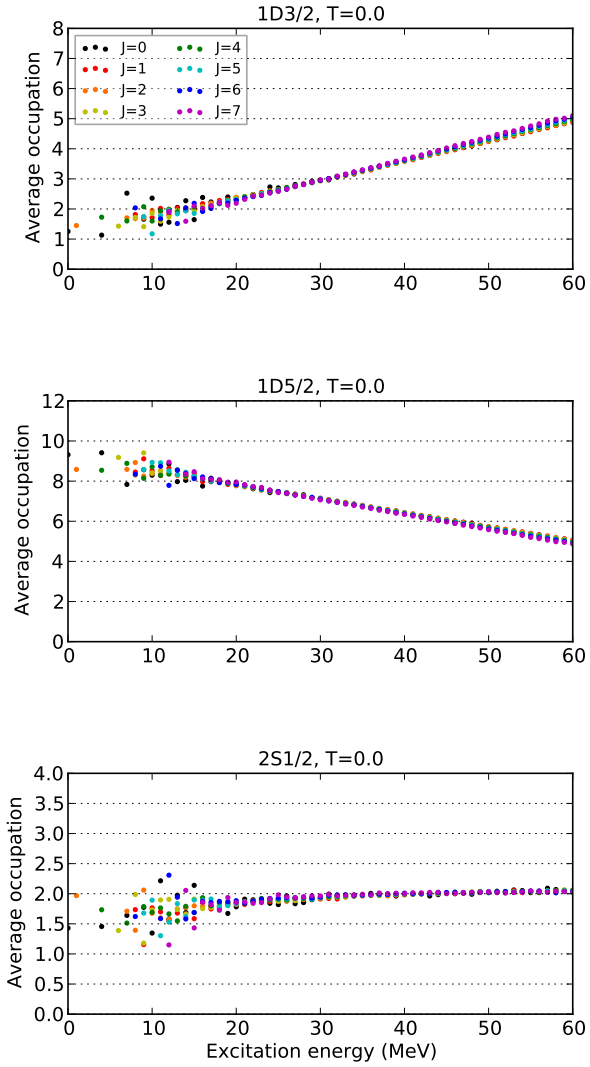

Figure 3.4: ^{28}Si single particle state occupation for states with isospin T= 0. The occupation numbers are the sum of protons and neutrons. The linear dependence of the d orbital occupation numbers on excitation energy is easily understood to arise from the spin-orbit splitting and particle-hole repulsion energies of those orbitals. This dependence is consistent across all values of T, although the intercepts of the d orbitals do shift as T increases.

is split evenly between protons and neutrons, giving a slope for each species of 1 particle per 24 MeV. Perhaps, then, the assumption in [24] that the single particle distributions are all similar to the ground state can be simply revised to say that above a certain nuclear excitation energy, the single particle distributions change only very slowly with excitation energy, resulting ultimately in similarly slowly changing strength distributions. This leaves us to challenge the second assumption in that work: that the transition energy of the GT resonance does not change with nuclear excitation energy.

From the ground state, nuclear transitions are dominated by the spin flip single particle transition, as is clear from comparing the strength distribution and the ground state single particle distribution; this results in the observed resonance. However, at higher excitation energies there is an abundance of final nuclear states that are reachable by the other single particle transitions, which has the consequence of leaving the daughter nucleus at similar or lower excitation. Thus, the GT resonance changes, distributing its strength to lower transition energy. Unfortunately, as can be seen in Figs. 3.5 and 3.6, there does not seem to be any obvious correlation between the single particle state energies and the peaks in the strength distributions. Nevertheless, given that single particle state occupations vary slowly with excitation energy, it is unsurprising that over a broad range of excitation energies (above the turmoil near the ground state and where the density of states is sufficiently high), the strength distributions are largely independent of excitation.

3.5.2 ^{28}Ne

The two biggest weaknesses of ^{28}Si as a model are that it is light and neutron poor. Unfortunately, current computational limits do not allow for careful examination of appropriately large nuclei, but we can hope to learn something by studying neutron rich light nuclei. Although ^{28}Ne has fewer sd shell configurations than ^{28}Si (it has only 2 protons and 2 neutron holes), it is nevertheless interesting because has proton fraction of $\approx$0.36; this is still neutron poor by supernova core standards, but not as grossly so as ^{28}Si.

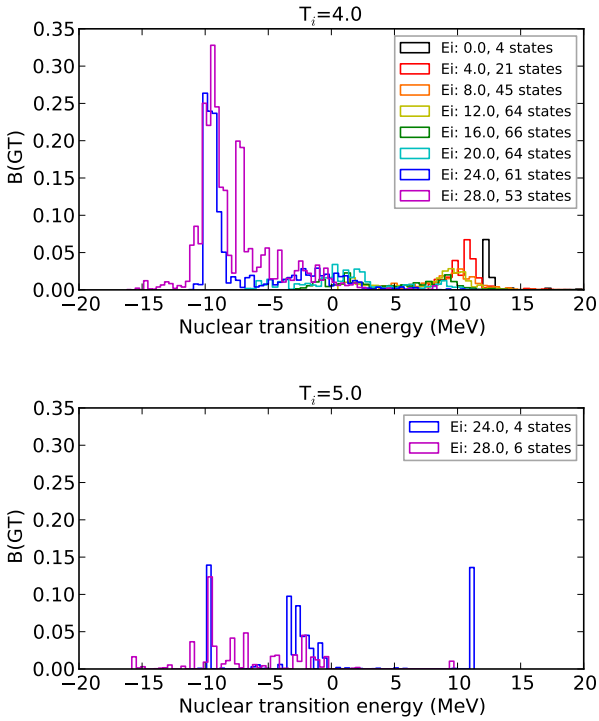

Figure 3.5: ^{28}Ne GT strength distribution. It is surprising that much of the strength at high excitation is concentrated 0 transition energy; this coupled with the fact that ^{28}Ne is very neutron rich imply an enhanced electron capture rate. We must be circumspect, however, as the model space for this nucleus is highly restricted.

Fig. 3.5 shows the GT strength distribution for ^{28}Ne. Interestingly, at high excitation, the strength is very strongly concentrated near zero transition energy. But this is a severely restricted model space, so we should exercise caution in interpreting the results.

3.5.3 ^{28}Na

At high excitation energies, nucleons will be promoted out of the core and into the valence sd shell and/or promoted from the sd shell into the fp shell. Here we propose a simple model accounting for one each of these promotions in ^{28}Ne: a proton leaving the core and entering the sd shell, and a neutron leaving the sd

shell and entering the fp shell. Although the core is now somewhat unrealistic in the context of sd shell computations (having a proton hole), the valence sd shell is exactly like ^{28}Na. These promotions roughly correspond to the behavior of real nuclei, and we gain the computational advantage of opening up phase space for more sd shell configurations, allowing for more realistic (sd shell only) computations.

Fig. 3.6 shows the strength distribution for ^{28}Na. Here the non-correlation with single particle energies is especially apparent; there are at least three peaks, with a fourth appearing near -10 MeV transition energy when $T_i = 4$ and $E_i = 28$ MeV. Unfortunately, this dashes any hope of finding a simple relationship between single particle energies and GT strength distribution, and we are relegated to considering strength as a function of isospin.

3.6 Computation of Transition Rate

Throughout this section, we will use natural units such that $\hbar = c = k_B = 1$. Following FFNI, the electron capture rate for a given initial nuclear state is

$$\lambda_{if} = \ln(2)\frac{f_{if}(T, \mu_e)}{(ft)_{if}} \tag{3.8}$$

where $(ft)_{if}$ is the comparative Gamow-Teller half-life computed from the matrix elements by

$$\log(ft^{GT}_{if}) = 3.596 - \log(|M^{GT}_{if}|^2) \tag{3.9}$$

$$\log(ft^{F}_{if}) = 3.791 - \log(|M^{F}_{if}|^2) \tag{3.10}$$

$$\frac{1}{(ft)_{if}} = \frac{1}{ft^{GT}_{if}} + \frac{1}{ft^{F}_{if}} \tag{3.11}$$

and $f_{if}(T, \mu_e)$ is the phase space integral for the incoming electron and outgoing neutrino. T is the temperature, and μ_e is the electron Fermi energy, including rest mass. The phase space integral is

$$f_{if} = \int_{w_l}^{\infty} w^2(w-q)^2 G(Z,w) f_e(w, \mu_e, T)(1 - f_\nu) dw \tag{3.12}$$

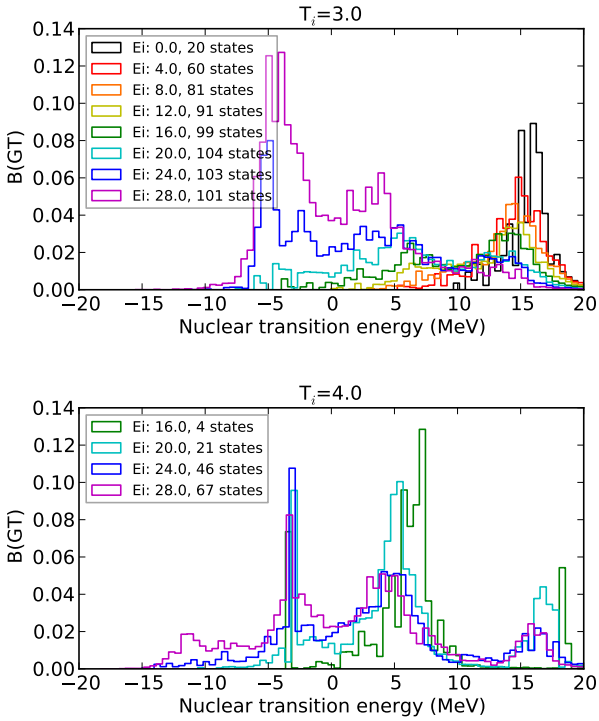

Figure 3.6: Strength distribution for ^{28}Na. Within the sd shell, this nucleus is identical to ^{28}Ne with one proton promoted out of the core and one neutron promoted into the fp shell, a configuration that will more closely match actual nuclei with very high excitations.

where w is the total electron energy in units of electron mass, q is the change in total nuclear energy $M_f + E_f - M_i - E_i$ in units of electron mass, Z is the nuclear charge, and f_e and f_ν are the electron and neutrino distribution functions. The lower limit w_l is a function of q, as the incoming electron must supply enough energy to the nucleus to make the transition; if q<1, then w_l=1 (corresponding to zero electron kinetic energy), while if q>1, w_l=q. G is related to the Coulomb barrier factor and is detailed in FFNI; rather than use the limiting approximations described in that work, we use the form given by eqn. 5b therein. Note that that work defines q in the negative sense of its use here; that is to say, q in that work is defined as the parent energy minus the daughter energy.

Up until neutrino trapping sets in at $\rho \sim 10^{12}$ g/cm^3, we may take $f_\nu \approx 0$. Here $f_e(w, \mu_e, T)$ is the Fermi-Dirac distribution $(1 + e^{(wm_e - \mu_e)/T})^{-1}$. Using this and our definition of w_l and integrating over final states, we at last arrive at

$$\lambda_i = \ln(2) \int_{-\infty}^{1} \left(\frac{B_i^{GT}(q)}{10^{3.596}} + \frac{B_i^{F}(q)}{10^{3.791}} \right) dq \int_{1}^{\infty} f_e(w, \mu_e, T) w^2 (w - q)^2 G(Z, w) dw$$
$$+\ln(2) \int_{1}^{\infty} \left(\frac{B_i^{GT}(q)}{10^{3.596}} + \frac{B_i^{F}(q)}{10^{3.791}} \right) dq \int_{q}^{\infty} f_e(w, \mu_e, T) w^2 (w - q)^2 G(Z, w) dw \quad (3.13)$$

To compute the total capture rate, we sum over population index weighted initial states.

$$\Lambda = \sum_i \lambda_i \frac{(2J_i + 1) e^{-E_i/T}}{G(T)} \quad (3.14)$$

where G is the partition function. Recall, however, that above ∼12 MeV, the strength distributions look similar. Therefore, we propose a modification to the GT Brink-Axel hypothesis by applying a cutoff energy below which all states are included weighted by their population index, and with all remaining statistical weight carried by a single high energy average state. This is in contrast to the FFN approach of placing the bulk of the strength in a single resonant transition that is identical for all states. In other words, where FFN treated all states as having an identical giant GT resonance, we treat all states above the cutoff energy as having exactly the same distribution. The difference in these two treatments is profound; Fig. 3.7 shows the strength distributions in the ground state for the FFN approach and the shell model; the large peak in the FFN distribution is the

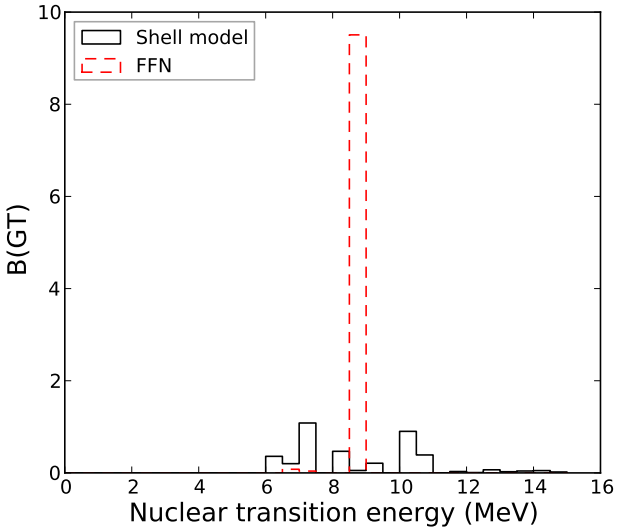

Figure 3.7: ^{28}Si ground state strength distribution. The solid line shows the distribution using our shell model calculations, and the dotted line shows the strength from the FFN prescription. The large peak in the FFN distribution is the GT resonance used in those works.

GT resonance. The two major differences are that the shell model result has less total strength, and the strength is spread to lower transition energies; the former will have the effect of decreasing the capture rate, while the latter will tend to increase it.

Despite the overestimate of the total strength and the misplacement of the resonance, the power of FFN is that it used experimental strengths wherever they were available, and any other technique of computing rates would be well-served by following that example. Therefore, the strength distributions that we ultimately use to compute capture rates are defined as follows. For the experimentally measured states used by FFN, we use the FFN strength distributions, but neglect the resonances. We then sum the strength, and remove that much from the low transition energy end of the strength distribution of our corresponding shell model state. We then augment the FFN distribution with what remains of the shell model distribution for that state. In essence, this gives a better estimate of both the capture strength sum rule and the (non-experimental) strength distribution. For higher energies, we simply used our shell model distributions, ignoring all parent shell

model states with an excitation energy lower than the highest used experimental state.

We now require the nuclear partition function to obtain appropriate initial state occupation indexes. There are a few approaches to the partition function problem, but in our case, the simplest and most self-consistent is to include only the sd shell states, *i.e.* only include in the partition function those states that can be constructed from configurations in the sd shell. The biggest weaknesses of this approach are that at high enough energies, the density of shell model states actually *decreases* to zero, and all negative parity states are neglected, as well as any other states that include configurations with one or more particles promoted into or out of the sd shell. By the same token, those states will also not be considered to contribute to the electron capture rate, thereby compensating for the overestimate of the included states's occupation indexes. With the partition function in hand, we can compute the total capture rate from eqn. 3.14.

The electron distribution function consists of two qualitatively different domains: when $1 \leq w \leq \mu_e/m_e$, it varies slowly from a maximum of at most 1 at $w = 1$ down to a minimum of 0.5 at $w = \mu_e/m_e$ (we will call this the "shoulder"), and when $w > \mu_e/m_e$, it is exponentially damped ("tail"). We numerically integrated the inner integrals of eqn. 3.13 using a combination of two methods, one for each domain. When the shoulder was part of the integration domain (*i.e.*, $q < \mu_e/m_e$), we integrated the shoulder with a 64-point Gauss-Legendre quadrature. Some or all of the tail is aways in the integration domain, and we integrated it with a 64-point Gauss-Laguerre quadrature.

Fig. 3.8 shows electron capture rates for ^{28}Si as a function of electron Fermi energy and temperature. The solid lines were computed using a cutoff energy of 12 MeV and a high energy average state strength distribution computed from the spin-weighted $(2J + 1)$ average of every state between 12 and 14 MeV, and the dashed lines are the rates computed using the FFN resonance prescription. At sufficiently high Fermi energy, there are enough electrons above the GT resonance used in the FFN approach for the rates to outstrip those of our shell model results, as the large amount of strength in the resonance outcompetes the shell model. However,

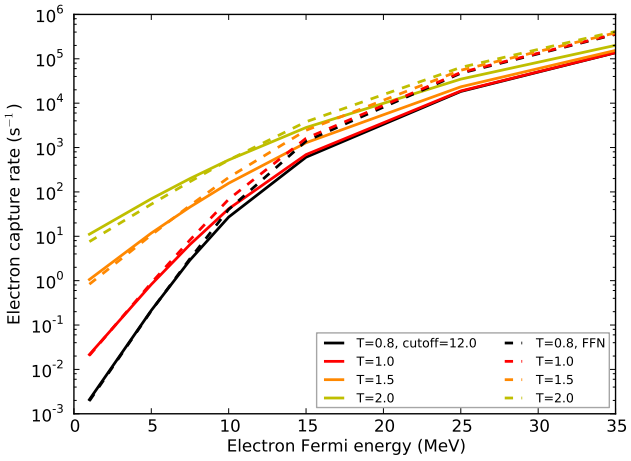

Figure 3.8: Electron capture rates for ^{28}Si as a function of density and temperature. Solid lines show rates with all states up to 12 MeV considered individually and the rest of the statistical weight carried by a single high energy average state, while dashed lines correspond to the rates when all states are assumed to have the same narrow GT resonance, in accordance with the FFN approach to the GT Brink-Axel hypothesis.

at low Fermi energy, the spread of strength to low transition energies found in the shell model approach serves to boost the rates above the FFN estimates.

Fig. 3.9 compares the shell model capture rates with a cutoff of 12 MeV against a GT Brink-Axel approach (as in Fig. 3.8), but with the single resonance in the FFN model replaced by the shell model strength distribution for the ground state. That is, in the "Brink" approach here, we used experimental values of the transition strength for each initial state where known, and the rest of the strength in each excited state is carried by the ground state distribution. In contrast to the behavior of the FFN approach, the shell model Brink-Axel curves lack the marked jump above the more comprehensive shell model rates as Fermi energy increases, and they eventually converge. It is notable that the GT Brink-Axel results are not uniformly greater *or* lesser than the more comprehensive shell model rates; in the Fermi energy region between 5 and 15 MeV, the T=0.8 and 1.0 MeV Brink-Axel rates just peek above the corresponding shell model rates.

In light of the apparent sensitivity to how excited states are handled in rate calculations, we compare in Fig. 3.10 the *thermodynamically unweighted* capture

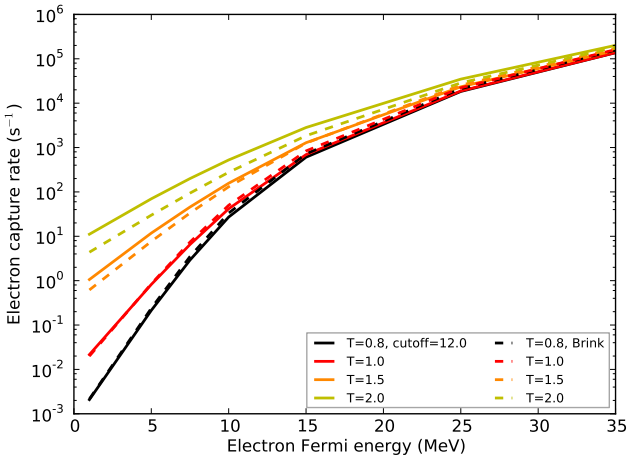

Figure 3.9: Electron capture rates for ^{28}Si as a function of density and temperature. Solid lines show rates with all states up to 12 MeV considered individually and the rest of the statistical weight carried by a single high energy average state, while dashed lines correspond to the rates when all states are assumed to have the same bulk GT strength distribution as our shell model calculation of the ground state.

rates of the high energy average (HEA) state for a range of cutoff energies. The solid lines show rates for an HEA state including all shell model states between 12 and 14 MeV, as in the previous calculations. The dashed lines give the rates of an HEA state computed from all states between 15 and 16 MeV, and the dotted lines are for an HEA state comprised of states between 20 and 20.3 MeV. The widths for the averaging were chosen such that each HEA state was comprised of at least 50 individual states.

The rates for all three HEA states differ from one another by at the most a factor of 3 in the range considered, which is offset by the reduction in statistical weight carried by the HEA state as the cutoff energy increases. The HEA statistical weight is simply the remaining probability after the occupation indexes of all lower-energy states are accounted for:

$$w_{HEA} = 1 - \frac{1}{G(T)} \sum_{E_i < E_{cutoff}} e^{-E_i/T} \tag{3.15}$$

The weights for the given cutoff energies and temperatures are shown in Table 3.1. Over most of the temperature range, the weight falls off much faster than

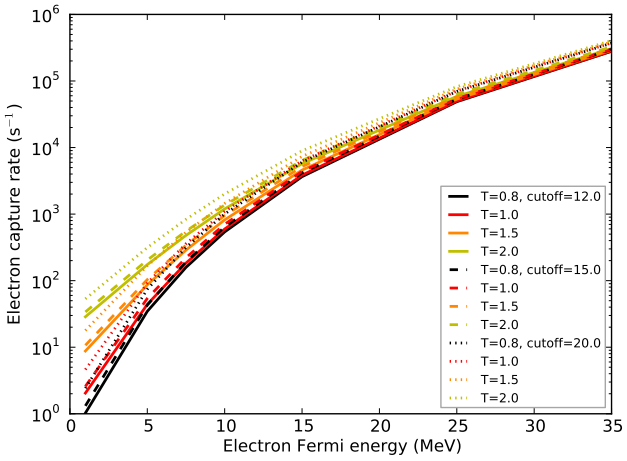

Figure 3.10: Thermodynamically unweighted electron capture rates for high energy average states in ^{28}Si. The solid lines are the rates for an HEA state with a cutoff energy of 12 MeV, the dashed lines show a cutoff of 15 MeV, and the dotted lines are for a cutoff of 20 MeV.

Table 3.1: Statistical weights of the high energy average state as a function of temperature and cutoff energy.

T (MeV)	Cutoff = 12 MeV	15 MeV	20 MeV
0.8	2.86×10^{-5}	1.70×10^{-6}	1.23×10^{-8}
1.0	6.30×10^{-4}	7.76×10^{-5}	1.88×10^{-6}
1.5	3.49×10^{-2}	1.11×10^{-2}	1.31×10^{-3}
2.0	2.00×10^{-1}	9.94×10^{-2}	2.53×10^{-2}

the unweighted HEA rate grows with cutoff energy. Fig. 3.11 shows the total capture rates for cutoff energies of 12 and 15 MeV. Clearly, the two choices produce nearly identical results, and the errors introduced by a particular choice of cutoff energy will ultimately be washed out by other uncertainties, including the eventual treatment of quenching

3.7 Discussion and Conclusions

The three principle observations from this work are that 1) at high excitation energies the GT strength distribution does not depend sensitively on nuclear excitation energy (though it is a function of isospin), 2) the GT strength distribu-

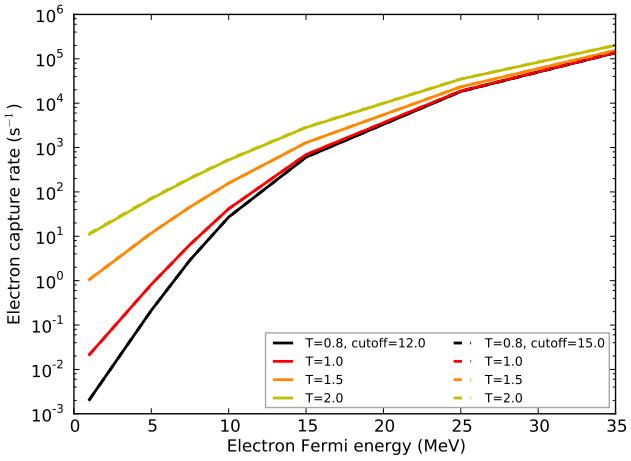

Figure 3.11: Electron capture rates for ^{28}Si comparing two choices of cutoff energy. The solid lines correspond to a cutoff energy of 12 MeV, wile the dashed lines are for a cutoff of 15 MeV. That they are nearly identical lends credence to the technique of using a high energy average state.

tion spreads to low and negative transition energies, and 3) the spreading of the strength tends to increase the electron capture rate, as not only does it decrease the electron energy capture threshold, but for a given incoming electron, it also increases the phase space of the outgoing neutrino.

As seen in Figs. 3.8 and 3.9, point 3 above is counteracted in some regimes of temperature and Fermi energy. In order to understand why the Brink-Axel rate sometimes exceeds the shell model rate, we must examine what the total strength, *i.e.* sum rule, looks like as a function of excitation energy. Fig. 3.12 shows the total GT strength vs. excitation energy for our shell model states, with each point corresponding to a single initial state. The vertical stripes are due to sampling; all shell model states up to 20 MeV are included, as are many states near 24 and 28 MeV. The black line shows the average total strength for all shown states in 1 MeV bins.

Comparing Figs. 3.7 and 3.12 we see that the strength in the GT resonance employed by FFN is about twice that computed from the shell model, resulting in an overestimate of the capture rate at high Fermi energies. The sources of the deviations in the shell model Brink-Axel approach are a little more subtle. Where

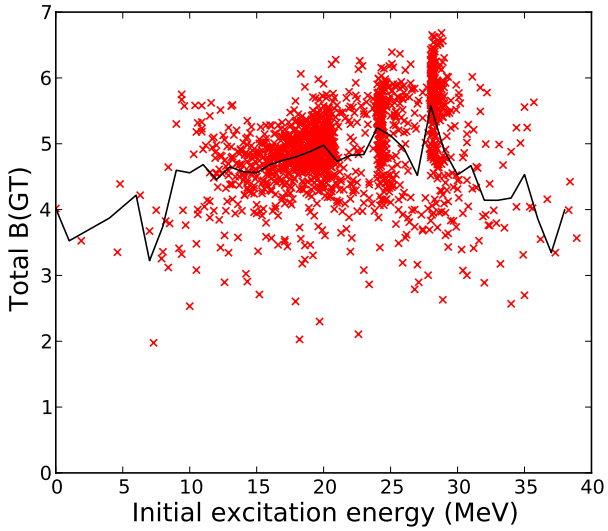

Figure 3.12: Total GT strength in ^{28}Si as a function of excitation energy. Each point corresponds to a specific state computed from the shell model, giving a GT sum rule for that state. The black line shows the average total strength, computed from 1 MeV bins.

the Brink-Axel rates are lower than the shell model rates, we easily attribute it to the low-lying strength of the excited states. Furthermore, it is apparent from Fig. 3.12 that on average, the total strength increases slowly with excitation (roughly, from $\sim$4 in the ground state to $\sim$5.5 at 30 MeV). But at relatively low excitation energies, there are two significant drops in the total strength, which account for the regions where the Brink-Axel rate exceeds the shell model rate. Recall that the GT Brink-Axel approach treats *all* excited states as having the same bulk GT strength distribution as the ground state, but the more comprehensive model includes contributions from those states that have less total strength. Importantly, some of those states are at low excitation. Hence, they do not have the low-lying strength seen in higher states, and they have a comparatively large Boltzmann factor. Consequently, there are temperature and Fermi energy regimes where the Brink-Axel approach overestimates the rate.

Ultimately, we must conclude that the GT Brink-Axel hypothesis as it has been traditionally used is likely inappropriate for obtaining accurate electron capture rates – and by extension, all nuclear weak rates – at the high temperatures

and densities characteristic of collapsing supernova cores. We must be circumspect, however, as the nuclei examined here are very light by supernova core standards. *If* later work is able to demonstrate that the trends found here are applicable to larger nuclei, then we will have found a useful technique for simplifying the accurate computation of weak rates in those nuclei.

The analysis of ^{28}Si in this work is essentially a cruder version of the work of Oda et al. We performed no careful matching of the energies of the daughter states relative to the parent states, meaning that where experimental data were not used, the distributions shown here will not have precise transition energies. This imprecision is unimportant for the sake of our goal here, which was to demonstrate the failure of the GT Brink-Axel hypothesis and how it can be modified for use at high initial excitation. With these results and the 20 years of experimental data collected since the Oda et al rate survey, though, it is worth re-examining the weak rate calculations for sd-shell nuclei, which are important in the late phases of stellar evolution leading up to core collapse.

This leaves us with two major directions to follow up. First, we will recompute the weak rates for all sd-shell nuclei over a wide range of temperatures and densities relevant to late stellar evolution and core collapse using our modification to the GT Brink-Axel hypothesis and the most recent experimental data. Second, we will seek ways to extend the results presented in this paper to the large, neutron-rich nuclei that are abundant during collapse, ideally allowing for more accurate computations of weak rates in those nuclei.

Chapter 3, in full, is material currently in preparation for publication in an academic journal with co-authors George M. Fuller, B. Alex Brown, and Calvin W. Johnson. I am the primary investigator and author of this paper.

Bibliography

[1] K. A. van Riper and J. M. Lattimer, "Stellar core collapse. I - Infall epoch," *Astrophys. J.*, vol. 249, pp. 270–289, Oct. 1981.

[2] K. A. van Riper, "Stellar core collapse. II - Inner core bounce and shock propagation," *Astrophys. J.*, vol. 257, pp. 793–820, June 1982.

[3] R. Bowers and J. R. Wilson, "Collapse of iron stellar cores," *Astrophys. J.*, vol. 263, pp. 366–376, Dec. 1982.

[4] J. M. Blondin, A. Mezzacappa, and C. DeMarino, "Stability of Standing Accretion Shocks, with an Eye toward Core-Collapse Supernovae," *Astrophys. J.*, vol. 584, pp. 971–980, Feb. 2003.

[5] J. M. Blondin and A. Mezzacappa, "Pulsar spins from an instability in the accretion shock of supernovae," *Nature*, vol. 445, pp. 58–60, Jan. 2007.

[6] L. Scheck, H.-T. Janka, T. Foglizzo, and K. Kifonidis, "Multidimensional supernova simulations with approximative neutrino transport. II. Convection and the advective-acoustic cycle in the supernova core," *Astronomy and Astrophysics*, vol. 477, pp. 931–952, Jan. 2008.

[7] T. D. Brandt, A. Burrows, C. D. Ott, and E. Livne, "Results from Core-collapse Simulations with Multi-dimensional, Multi-angle Neutrino Transport," *Astrophys. J.*, vol. 728, p. 8, Feb. 2011.

[8] A. Arcones, H.-T. Janka, and L. Scheck, "Nucleosynthesis-relevant conditions in neutrino-driven supernova outflows. I. Spherically symmetric hydrodynamic simulations," *Astronomy and Astrophysics*, vol. 467, pp. 1227–1248, June 2007.

[9] W. R. Hix, E. J. Lentz, M. Baird, O. E. B. Messer, A. Mezzacappa, C.-T. Lee, S. W. Bruenn, J. M. Blondin, and P. Marronetti, "Understanding Core-Collapse Supernovae," *Nuclear Physics A*, vol. 834, pp. 602–607, Mar. 2010.

[10] H. A. Bethe, G. E. Brown, J. Applegate, and J. M. Lattimer, "Equation of state in the gravitational collapse of stars," *Nuclear Physics A*, vol. 324, pp. 487–533, July 1979.

[11] J. N. Bahcall, S. B. Treiman, and A. Zee, "Neutral currents and stellar cooling," *Physics Letters B*, vol. 52, pp. 275–278, Oct. 1974.

[12] D. A. Dicus, E. W. Kolb, D. N. Schramm, and D. L. Tubbs, "Neutrino pair bremsstrahlung including neutral current effects," *Astrophys. J.*, vol. 210, pp. 481–488, Dec. 1976.

[13] G. M. Fuller and B. S. Meyer, "High-temperature neutrino-nucleus processes in stellar collapse," *Astrophys. J.*, vol. 376, pp. 701–716, Aug. 1991.

[14] G. W. Misch, B. A. Brown, and G. M. Fuller, "Neutrino-pair emission from hot nuclei during stellar collapse," *Phys. Rev. C*, vol. 88, p. 015807, July 2013.

[15] H. A. Bethe, "An Attempt to Calculate the Number of Energy Levels of a Heavy Nucleus," *Physical Review*, vol. 50, pp. 332–341, Aug. 1936.

[16] G. M. Fuller, "Neutron shell blocking of electron capture during gravitational collapse," *Astrophys. J.*, vol. 252, pp. 741–764, Jan. 1982.

[17] K. Langanke and G. Martínez-Pinedo, "Rate Tables for the Weak Processes of pf-SHELL Nuclei in Stellar Environments," *Atomic Data and Nuclear Data Tables*, vol. 79, pp. 1–46, Sept. 2001.

[18] R. D. Woods and D. S. Saxon, "Diffuse Surface Optical Model for Nucleon-Nuclei Scattering," *Physical Review*, vol. 95, pp. 577–578, July 1954.

[19] O. Haxel, J. H. Jensen, and H. E. Suess, "On the "Magic Numbers" in Nuclear Structure," *Physical Review*, vol. 75, pp. 1766–1766, June 1949.

[20] M. G. Mayer, "Nuclear Configurations in the Spin-Orbit Coupling Model. I. Empirical Evidence," *Physical Review*, vol. 78, pp. 16–21, Apr. 1950.

[21] M. G. Mayer, "Nuclear Configurations in the Spin-Orbit Coupling Model. II. Theoretical Considerations," *Physical Review*, vol. 78, pp. 22–23, Apr. 1950.

[22] A. Deshalit, H. Feshbach, and E. Sheldon, "Theoretical Nuclear Physics Vol. 1: Nuclear Structure," *Physics Today*, vol. 27, p. 215, 1974.

[23] G. M. Fuller, W. A. Fowler, and M. J. Newman, "Stellar weak-interaction rates for sd-shell nuclei. I - Nuclear matrix element systematics with application to Al-26 and selected nuclei of importance to the supernova problem," *Astrophys. J. (Supplement)*, vol. 42, pp. 447–473, Mar. 1980.

[24] G. M. Fuller, W. A. Fowler, and M. J. Newman, "Stellar weak interaction rates for intermediate-mass nuclei. II - A = 21 to A = 60," *Astrophys. J.*, vol. 252, pp. 715–740, Jan. 1982.

[25] G. M. Fuller, W. A. Fowler, and M. J. Newman, "Stellar weak interaction rates for intermediate mass nuclei. III - Rate tables for the free nucleons and nuclei with A = 21 to A = 60," *Astrophys. J. (Supplement)*, vol. 48, pp. 279–319, Mar. 1982.

[26] G. M. Fuller, W. A. Fowler, and M. J. Newman, "Stellar weak interaction rates for intermediate-mass nuclei. IV - Interpolation procedures for rapidly varying lepton capture rates using effective log (ft)-values," *Astrophys. J.*, vol. 293, pp. 1–16, June 1985.

[27] E. W. Kolb and T. J. Mazurek, "Production and inelastic scattering of neutrinos by nuclei at extreme temperatures," *Astrophys. J.*, vol. 234, pp. 1085–1093, Dec. 1979.

[28] C. J. Horowitz, "Density dependence of nuclear neutrino-pair production," *Physical Review Letters*, vol. 69, pp. 2627–2630, Nov. 1992.

[29] W. D. Arnett, "Neutrino trapping during gravitational collapse of stars," *Astrophys. J.*, vol. 218, pp. 815–833, Dec. 1977.

[30] H. A. Bethe and J. R. Wilson, "Revival of a stalled supernova shock by neutrino heating," *Astrophys. J.*, vol. 295, pp. 14–23, Aug. 1985.

[31] M. Liebendörfer, T. Fischer, C. Fröhlich, W. R. Hix, K. Langanke, G. Martinez-Pinedo, A. Mezzacappa, S. Scheidegger, F.-K. Thielemann, and S. C. Whitehouse, "Nuclear physics in core-collapse supernovae," *New Astronomy Reviews*, vol. 52, pp. 373–376, Oct. 2008.

[32] M. Liebendörfer, T. Fischer, M. Hempel, A. Mezzacappa, G. Pagliara, I. Sagert, J. Schaffner-Bielich, S. Scheidegger, F.-K. Thielemann, and S. C. Whitehouse, "Supernovae as Nuclear and Particle Physics Laboratories," *Nuclear Physics A*, vol. 827, pp. 573–578, Aug. 2009.

[33] N. J. Hammer, H.-T. Janka, and E. Müller, "Three-dimensional Simulations of Mixing Instabilities in Supernova Explosions," *Astrophys. J.*, vol. 714, pp. 1371–1385, May 2010.

[34] A. Burrows, J. C. Dolence, and J. W. Murphy, "An Investigation into the Character of Pre-Explosion Core-Collapse Supernova Shock Motion," *ArXiv e-prints*, Apr. 2012.

[35] D. L. Tubbs and D. N. Schramm, "Neutrino Opacities at High Temperatures and Densities," *Astrophys. J.*, vol. 201, pp. 467–488, Oct. 1975.

[36] D. L. Tubbs, "Conservative scattering, electron scattering, and neutrino thermalization," *Astrophys. J.*, vol. 231, pp. 846–853, Aug. 1979.

[37] G. Beaudet, V. Petrosian, and E. E. Salpeter, "Energy Losses due to Neutrino Processes," *Astrophys. J.*, vol. 150, p. 979, Dec. 1967.

[38] Z. Barkat, "Neutrino processes in stellar interiors," *Annual Reviews Astronomy and Astrophysics*, vol. 13, pp. 45–68, 1975.

[39] N. Itoh and Y. Kohyama, "Neutrino-pair bremsstrahlung in dense stars. I - Liquid metal case," *Astrophys. J.*, vol. 275, pp. 858–866, Dec. 1983.

[40] P. J. Schinder, D. N. Schramm, P. J. Wiita, S. H. Margolis, and D. L. Tubbs, "Neutrino emission by the pair, plasma, and photo processes in the Weinberg-Salam model," *Astrophys. J.*, vol. 313, pp. 531–542, Feb. 1987.

[41] N. Itoh, T. Adachi, M. Nakagawa, Y. Kohyama, and H. Munakata, "Neutrino energy loss in stellar interiors. III - Pair, photo-, plasma, and bremsstrahlung processes," *Astrophys. J.*, vol. 339, pp. 354–364, Apr. 1989.

[42] Y. Kohyama, N. Itoh, A. Obama, and H. Mutoh, "Neutrino energy loss in stellar interiors. V - Recombination neutrino process," *Astrophys. J.*, vol. 415, pp. 267–277, Sept. 1993.

[43] N. Itoh, A. Nishikawa, and Y. Kohyama, "Neutrino Energy Loss in Stellar Interiors. VIII. Braaten-Segel Approximation for the Plasma Neutrino Process," *Astrophys. J.*, vol. 470, p. 1015, Oct. 1996.

[44] N. Itoh, H. Hayashi, A. Nishikawa, and Y. Kohyama, "Neutrino Energy Loss in Stellar Interiors. VII. Pair, Photo-, Plasma, Bremsstrahlung, and Recombination Neutrino Processes," *Astrophys. J. (Supplement)*, vol. 102, p. 411, Feb. 1996.

[45] E. G. Flowers, P. G. Sutherland, and J. R. Bond, "Neutrino pair bremsstrahlung by nucleons in neutron-star matter," *Phys. Rev. D*, vol. 12, pp. 315–318, July 1975.

[46] S. Reddy, M. Prakash, and J. M. Lattimer, "Neutrino interactions in hot and dense matter," *Phys. Rev. D*, vol. 58, p. 013009, July 1998.

[47] M. Prakash, J. M. Lattimer, R. F. Sawyer, and R. R. Volkas, "Neutrino Propagation in Dense Astrophysical Systems," *Annual Review of Nuclear and Particle Science*, vol. 51, pp. 295–344, 2001.

[48] S. W. Bruenn and W. C. Haxton, "Neutrino-nucleus interactions in core-collapse supernovae," *Astrophys. J.*, vol. 376, pp. 678–700, Aug. 1991.

[49] J. M. Sampaio, K. Langanke, G. Martínez-Pinedo, and D. J. Dean, "Neutral-current neutrino reactions in the supernova environment," *Physics Letters B*, vol. 529, pp. 19–25, Mar. 2002.

[50] G. Martínez-Pinedo, "Nuclear physics aspects of supernovae evolution and nucleosynthesis," *Journal of Physics G Nuclear Physics*, vol. 35, p. 014057, Jan. 2008.

[51] K. Langanke, G. Martínez-Pinedo, B. Müller, H.-T. Janka, A. Marek, W. R. Hix, A. Juodagalvis, and J. M. Sampaio, "Effects of Inelastic Neutrino-Nucleus Scattering on Supernova Dynamics and Radiated Neutrino Spectra," *Physical Review Letters*, vol. 100, p. 011101, Jan. 2008.

[52] B. A. Brown, A. Etchegoyen, N. S. Godwin, W. D. M. Rae, W. Richter, W. E. Ormand, E. K. Warburton, J. S. Winfield, L. Zhao, and C. H. Zimmerman, "Oxbash for windows," *MSU-NSCL Report No. 1289*, 2004.

[53] B. A. Brown and W. A. Richter, "New "USD" Hamiltonians for the sd shell," *Phys. Rev. C*, vol. 74, p. 034315, Sept. 2006.

[54] M. Honma, T. Otsuka, B. A. Brown, and T. Mizusaki, "New effective interaction for pf -shell nuclei and its implications for the stability of the N=Z=28 closed core," *Phys. Rev. C*, vol. 69, p. 034335, Mar. 2004.

[55] B. A. Brown, W. D. M. Rae, E. McDonald, and M. Horoi 2012.

[56] B. A. Brown and B. H. Wildenthal, "Status of the nuclear shell model," *Annual Review of Nuclear and Particle Science*, vol. 38, no. 1, pp. 29–66, 1988.

[57] G. Martínez-Pinedo, A. Poves, E. Caurier, and A. P. Zuker, "Effective g_A in the pf shell," *Phys. Rev. C*, vol. 53, p. 2602, June 1996.

[58] A. Arima, K. Shimizu, W. Bentz, and H. Hyuga *Advances in Nuclear Physics*, vol. 18, no. 1, 1987.

[59] I. S. Towner, "Quenching of spin matrix elements in nuclei," *Physics Reports*, vol. 155, pp. 263–377, Nov. 1987.

[60] A. Bohr and B. R. Mottelson, *Nuclear Structure*, vol. 1. World Scientific Publishing Co., 1998.

[61] G. Shen, S. Gandolfi, S. Reddy, and J. Carlson, "Spin Response and Neutrino Emissivity of Dense Neutron Matter," *ArXiv e-prints*, May 2012.

[62] B. Friman and O. Maxwell, "Neutrino emissivities of neutron stars," *The Astrophysical Journal*, vol. 232, pp. 541–557, 1979.

[63] D. M. Brink. PhD thesis, Oxford University, 1955.

[64] P. Axel, "Electric Dipole Ground-State Transition Width Strength Function and 7-Mev Photon Interactions," *Physical Review*, vol. 126, pp. 671–683, Apr. 1962.

[65] R. B. Firestone, *Table of Isotopes*. Wiley-Interscience, 1.0 ed., March 1996.

[66] K. Yako, H. Sakai, M. B. Greenfield, K. Hatanaka, M. Hatano, J. Kamiya, H. Kato, Y. Kitamura, Y. Maeda, C. L. Morris, H. Okamura, J. Rapaport, T. Saito, Y. Sakemi, K. Sekiguchi, Y. Shimizu, K. Suda, A. Tamii, N. Uchigashima, and T. Wakasa, "Determination of the Gamow Teller quenching factor from charge exchange reactions on ^{90}Zr," *Physics Letters B*, vol. 615, pp. 193–199, June 2005.

[67] K. Yako, M. Sasano, K. Miki, H. Sakai, M. Dozono, D. Frekers, M. B. Greenfield, K. Hatanaka, E. Ihara, M. Kato, T. Kawabata, H. Kuboki, Y. Maeda, H. Matsubara, K. Muto, S. Noji, H. Okamura, T. H. Okabe, S. Sakaguchi, Y. Sakemi, Y. Sasamoto, K. Sekiguchi, Y. Shimizu, K. Suda, Y. Tameshige, A. Tamii, T. Uesaka, T. Wakasa, and H. Zheng, "Gamow-Teller Strength Distributions in Sc48 by the Ca48(p,n) and Ti48(n,p) Reactions and Two-Neutrino Double-β Decay Nuclear Matrix Elements," *Physical Review Letters*, vol. 103, p. 012503, July 2009.

[68] D. Frekers, P. Puppe, J. H. Thies, and H. Ejiri, "Gamow-Teller strength extraction from (^{3}He, t) reactions," *Nuclear Physics A*, vol. 916, pp. 219–240, Oct. 2013.

[69] Extreme Light Infrastructure.

[70] M. B. Aufderheide, I. Fushiki, S. E. Woosley, and D. H. Hartmann, "Search for important weak interaction nuclei in presupernova evolution," *Astrophys. J. (Supplement)*, vol. 91, pp. 389–417, Mar. 1994.

[71] K. Kar, A. Ray, and S. Sarkar, "Beta-decay rates of FP shell nuclei with A greater than 60 in massive stars at the presupernova stage," *Astrophys. J.*, vol. 434, pp. 662–683, Oct. 1994.

[72] S. Chakravarti, K. Kar, A. Ray, and S. Sarkar, "Electron Capture Rates of Mid-fp Shell Nuclei for Supernova and Stellar Evolution," *ArXiv Astrophysics e-prints*, Oct. 1999.

[73] T. Kajino, E. Shiino, H. Toki, B. A. Brown, and B. H. Wildenthal, "Beta decay rates of sd-shell nuclei in stellar interiors," *Nuclear Physics A*, vol. 480, pp. 175–187, Mar. 1988.

[74] K. Langanke and G. Martinez-Pinedo, "Supernova electron capture rates for ^{55}Co and ^{56}Ni," *Physics Letters B*, vol. 436, pp. 19–24, Sept. 1998.

[75] E. Caurier, K. Langanke, G. Martínez-Pinedo, and F. Nowacki, "Shell-model calculations of stellar weak interaction rates. I. Gamow-Teller distributions and spectra of nuclei in the mass range A=45-65," *Nuclear Physics A*, vol. 653, pp. 439–452, July 1999.

[76] K. Langanke and G. Martínez-Pinedo, "Supernova electron capture rates on odd-odd nuclei," *Physics Letters B*, vol. 453, pp. 187–193, May 1999.

[77] G. Martinezpinedo and K. Langanke, "Supernova electron capture rates," *Nuclear Physics A*, vol. 654, p. 904, July 1999.

[78] K. Langanke and G. Martínez-Pinedo, "Shell-model calculations of stellar weak interaction rates: II. Weak rates for nuclei in the mass range /A=45-65 in supernovae environments," *Nuclear Physics A*, vol. 673, pp. 481–508, June 2000.

[79] A. L. Cole, T. S. Anderson, R. G. T. Zegers, S. M. Austin, B. A. Brown, L. Valdez, S. Gupta, G. W. Hitt, and O. Fawwaz, "Gamow-Teller strengths and electron-capture rates for pf-shell nuclei of relevance for late stellar evolution," *Phys. Rev. C*, vol. 86, p. 015809, July 2012.

[80] T. Fischer, K. Langanke, and G. Martínez-Pinedo, "Neutrino-pair emission from nuclear de-excitation in core-collapse supernova simulations," *Phys. Rev. C*, vol. 88, p. 065804, Dec. 2013.

[81] K. Langanke, E. Kolbe, and D. J. Dean, "Unblocking of the Gamow-Teller strength in stellar electron capture on neutron-rich germanium isotopes," *Phys. Rev. C*, vol. 63, p. 032801, Mar. 2001.

[82] G. Martínez-Pinedo, Y. H. Lam, K. Langanke, R. G. T. Zegers, and C. Sullivan, "Astrophysical weak-interaction rates for selected A =20 and A =24 nuclei," *Phys. Rev. C*, vol. 89, p. 045806, Apr. 2014.

[83] A. Juodagalvis, K. Langanke, W. R. Hix, G. Martínez-Pinedo, and J. M. Sampaio, "Improved estimate of electron capture rates on nuclei during stellar core collapse," *Nuclear Physics A*, vol. 848, pp. 454–478, Dec. 2010.

[84] J.-U. Nabi and M. Sajjad, "Comparative study of Gamow-Teller strength distributions in the odd-odd nucleus V50 and its impact on electron capture rates in astrophysical environments," *Phys. Rev. C*, vol. 76, p. 055803, Nov. 2007.

[85] J.-U. Nabi, "Neutrino cooling rates due to ^{54,55,56}Fe for presupernova evolution of massive stars," *Advances in Space Research*, vol. 48, pp. 985–997, Sept. 2011.

[86] J.-U. Nabi, "Nickel isotopes in stellar matter," *European Physical Journal A*, vol. 48, p. 84, June 2012.

[87] T. Oda, M. Hino, K. Muto, M. Takahara, and K. Sato, "Rate Tables for the Weak Processes of sd-Shell Nuclei in Stellar Matter," *Atomic Data and Nuclear Data Tables*, vol. 56, pp. 231–403, Mar. 1994.

[88] A. A. Dzhioev, A. I. Vdovin, V. Y. Ponomarev, J. Wambach, K. Langanke, and G. Martínez-Pinedo, "Gamow-Teller strength distributions at finite temperatures and electron capture in stellar environments," *Phys. Rev. C*, vol. 81, p. 015804, Jan. 2010.

[89] P. Sarriguren, "Stellar electron-capture rates in pf-shell nuclei from quasiparticle random-phase approximation calculations," *Phys. Rev. C*, vol. 87, p. 045801, Apr. 2013.